Phosphorus and nitrogen starvation reveal life-cycle specific responses in the metabolome of *Emiliania huxleyi* (Haptophyta)

Robin Wördenweber,[1] Sebastian D. Rokitta,[2] Elena Heidenreich,[3] Katrin Corona,[1] Frank Kirschhöfer,[3] Kirsten Fahl,[4] Jessica L. Klocke,[5] Tilman Kottke,[5] Gerald Brenner-Weiß,[3] Björn Rost,[2] Jan H. Mussgnug,[1] Olaf Kruse [1]*

[1]Algae Biotechnology & Bioenergy, Department of Biology, Center for Biotechnology (CeBiTec), Bielefeld University, Bielefeld, Germany
[2]Marine Biogeosciences, Alfred Wegener Institute, Helmholtz Centre for Polar and Marine Research, Bremerhaven, Germany
[3]Analytical Biochemistry, Department of Bioengineering and Biosystems, Institute of Functional Interfaces, Karlsruhe Institute of Technology, Eggenstein-Leopoldshafen, Germany
[4]Marine Geology and Paleontology, Alfred Wegener Institute, Helmholtz Centre for Polar and Marine Research, Bremerhaven, Germany
[5]Physical and Biophysical Chemistry, Department of Chemistry, Bielefeld University, Bielefeld, Germany

Abstract

The coccolithophore *Emiliania huxleyi* is a microalga with biogeochemical and biotechnological relevance, due to its high abundance in the ocean and its ability to form intricate calcium carbonate structures. Depletion of macronutrients in oceanic waters is very common and will likely enhance with advancing climate change. We present the first comprehensive metabolome study analyzing the effect of phosphorus (P) and nitrogen (N) starvation on the diploid and haploid life-cycle stage, applying various metabolome analysis methods to gain new insights in intracellular mechanisms to cope with nutrient starvation. P-starvation led to an accumulation of many generic and especially N-rich metabolites, including lipids, osmolytes, and pigments. This suggests that P-starvation primarily arrests cell-cycling due to lacking P for nucleic acid synthesis, but that enzymatic functionality is widely preserved. Also, the de-epoxidation ratio of the xanthophyll cycle was upregulated in the diploid stage under P-starvation, indicating increased nonphotochemical quenching, a response typically observed under high light stress. In contrast, N-starvation resulted in a decrease of most central metabolites, also P-containing ones, especially in the diploid stage, indicating that most enzymatic functionality ceased. The two investigated nutrient starvation conditions caused significantly different responses, contrary to previous assumptions derived from transcriptomic studies. Data highlight that instantaneous biochemical flux is a more dominant driver of the metabolome than the transcriptomically rearranged pathway patterns. Due to the fundamental nature of the observed responses it may be speculated that microalgae with similar nutrient requirements can cope better with P-starvation than with N-starvation.

The coccolithophore *Emiliania huxleyi* is a cosmopolitan marine microalga that forms an external shell consisting of elaborately shaped calcium carbonate platelets, so-called coccoliths. This alga drives a haplo-diplontic life-cycle, in which it can switch between a calcifying, diploid form and a non-calcifying, haploid flagellated swarmer cell (Paasche 2001).

Beyond its prominent role as a calcifier in the biogeochemistry of the oceans (Rost and Riebesell 2004), it is a promising organism for biotechnological purposes, as it contains diverse lipids, i.e., unique long-chained C_{37}-C_{39} lipids in the form of alkenones (Volkman et al. 1980; Eltgroth et al. 2005), as well as Ω-3 fatty acids incorporated into lipids, which are widely used as nutraceuticals (Abedi and Sahari 2014). Furthermore, *E. huxleyi* is heavily investigated with regard to the process of coccolith formation (Klaveness 1972; Paasche 1998; Young et al. 1999; Sviben et al. 2016). Because coccoliths are highly structured bio-composite materials, an understanding of their biogenesis could enable the industrial production of custom-designed micro-scale parts made of calcium carbonate and other materials (Holtz et al.

2013; Krumov and Posten 2013). *E. huxleyi* also possesses diverse pigments (Garrido et al. 2000), for instance, as a descendant of the red algal lineage (Falkowski et al. 2004), it contains chlorophyll *c* (Chl *c*) instead of Chl *b*. More than 50% (by mole) of *E. huxleyi*'s pigments are chlorophylls (Stolte et al. 2000). Furthermore, 19′-hexanoyloxy-4-ketofucoxanthin and other carotenoids are present in high amounts and are discussed as biosynthetic replacements for existing red food colors (Dewick 2001).

The recent publication of *E. huxleyi*'s genome (Read et al. 2013) has enabled broader genomic and transcriptomic approaches that have not only yielded new insights into the ecophysiology of this alga and its life-cycle stages (Rokitta et al. 2011, 2014, 2016; von Dassow et al. 2015), but have also promoted the establishment of this species as a new model organism for haptophyte microalgae (Read et al. 2013). Applications of different genomic, transcriptomic, proteomic, and metabolomic methodologies have led to increasingly detailed pictures of its cell physiology and metabolism (Jones et al. 2011; Rokitta et al. 2011, 2014, 2016; Bochenek et al. 2013; Jones et al. 2013; Obata et al. 2013; Mausz and Pohnert 2015; McKew et al. 2015; Zhang et al. 2016). However, as with all organisms, there is ongoing debate about the consistency and agreement between different methodologies targeting the different levels of biological organization and regulation, i.e., the genome, transcriptome, proteome, and metabolome (Feder and Walser 2005; Dettmer et al. 2007).

To make a first step in bridging this gap in *E. huxleyi*, here we applied an innovative combination of methods to assess abundances of key metabolites from different biochemical pathways and correlated the emerging picture with existing transcriptome data. As P- or N-starvation were clearly reached at the harvesting time point, the physiological state is comparable to the transcriptome study (late starvation just before cessation of growth), enabling us to correlate the here obtained metabolite profiles with gene expression patterns obtained previously (Rokitta et al. 2014, 2016). By combining basic data about metabolic budgets and physiological responses with transcript abundances, important insights are provided that are necessary for future numerical or Boolean models on different scales (Holtz et al. 2015; Knies et al. 2015). Given the common principles of cell biology of many unicellular organisms, knowledge about the basal functioning modes of these cells may be transferable to other biological systems and cell model implementations (Herrgård et al. 2008; Heinemann and Sauer 2010). For instance, the depletion of macronutrients is a frequent scenario in oceanic habitats. As a response, microalgae arrest their cellular growth and restructure their metabolism to maintain vital functions and secure survival, but minimize nutrient consumption. Consequently, microalgal responses to macronutrient starvation have often been investigated regarding the ecophysiology of these microbes. However, stagnating growth due to

nutrient starvation does not necessarily shut down calcification and thus often leads to a relative overproduction of coccoliths (Paasche 1998; Dyhrman et al. 2006), which is an interesting fact to biotechnologists that aim to exploit this biological function (Hariskos et al. 2016).

To investigate the cellular response to macronutrient starvation, transcriptomic, and proteomic studies have been conducted, applying starvation scenarios in nitrogen (N; Rokitta et al. 2014; McKew et al. 2015), phosphorus (P; McKew et al. 2015; Rokitta et al. 2016) and sulfur (Bochenek et al. 2013). In the studies carried out by Rokitta et al. (2014, 2016), it was found that in response to both N- and P-starvation, the transcriptome to a large extent experiences synonymous changes, because cells strongly down-regulate overall gene transcription, synthesis of proteins as well as photosynthesis and mitochondrial ATP generation. The transcriptomic data also hinted towards a major restructuring of metabolism, including decreased synthesis of nucleotide bases and amino acids, highly efficient recycling of the respective limiting nutrients, as well an intensified and rearranged lipid metabolism. The latter was attributed to the massive production of lipids under starvation (Eltgroth et al. 2005; Malitsky et al. 2016; Shemi et al. 2016).

To date comprehensive metabolic studies on *E. huxleyi* are very rare, and especially the haploid life-cycle stage is poorly investigated. Three previously conducted studies focus on the establishment of a GC-MS based metabolome analysis for a diploid life-cycle stage (Obata et al. 2013), analysis of metabolites in different growth phases for both life-cycle stages (Mausz and Pohnert 2015), or observing the effects of virus infection on a diploid life-cycle stage (Rosenwasser et al. 2014). In contrast, the study presented here is the first broad metabolome study focused on cellular alterations in response to nutrient starvation.

To analyze the effect of nutrient starvation, we grew diploid (2N) and haploid (1N) *E. huxleyi* life-cycle stages (RCC 1216 and RCC 1217, respectively) under macronutrient starvation scenarios (–P or –N). We then assessed various metabolites representative for diverse biochemical pathways by applying adapted gas chromatography-mass spectrometry (GC-MS), gas chromatography coupled to flame ionization detection (GC-FID), liquid chromatography with tandem mass spectrometry (LC-MS/MS), Fourier transform infrared spectroscopy (FTIR) as well as high-performance liquid chromatography (HPLC) based methods. Last, we investigated the degree of consistency with transcriptome analyses conducted previously in these microalgae (Rokitta et al. 2014, 2016).

Materials

Experimental setup

E. huxleyi RCC 1216 (diploid life-cycle stage, calcifying, 2N) and RCC 1217 (haploid life-cycle stage, non-calcifying,

1N) were grown in sterile filtered ESAW medium (Berges et al. 2001), either with replete nutrients or under nutrient starvation, induced by adding only 10% of the respective nutrient at the beginning of cultivation (nitrate: 549 μM or 54.9 μM, phosphate: 22.4 μM or 2.24 μM). ESAW medium was used instead of natural seawater to avoid potential natural fluctuation in medium composition. *E. huxleyi* has been previously shown to grow well in ESAW medium (Berges et al. 2001), and the diploid strain used in this study did not show any signs of ceasing calcification or unsteady growth over the course of > 12 months. Precultures were grown in replete medium in 100 mL shake flasks up to exponential growth phase and used as inoculum for the main cultures. Three biological replicates of each life-cycle stage were inoculated with 2000 cells mL^{-1} in 1 L Schott glass bottles containing sterile filtered medium with either replete, 10% nitrate or 10% phosphate. No headspace was left on the day of inoculation, but it increased daily by $\sim$4 mL due to sampling of cell numbers and nutrient analysis. Cultures were grown at 20°C under 300 μmol m^{-2} s^{-1} illumination with a 16 : 8 h light/dark cycle, and were shaken manually twice a day. The cell numbers were determined in triplicate via a Z2 Coulter® Particle Counter and Size Analyzer (Beckman Coulter). Axenity was ensured by pre-treating the stock cultures with kanamycin sulfate (0.5 mg mL^{-1}) and further monitoring at the beginning and end of the cultivation by microscopically checking the culture and plating aliquots onto ESAW and lysogeny broth agar plates (10 g L^{-1} bactotryptone, 5 g L^{-1} yeast extract, 10 g L^{-1} sodium chloride, 15 g L^{-1} agar, pH 7.0). Triplicate samples were taken for analysis of nutrients in the supernatant. Therefore culture was centrifuged at 4°C (14,000 $\times$ g, 2 min) and supernatants were frozen at -20°C until further analysis. Nutrient concentrations were determined using photometric tests for nitrate in seawater (Spectroquant®, Merck) and o-phosphate (Spectroquant®, Merck). The total alkalinity was measured with a photometric test according to Sarazin et al. (1999).

Metabolome harvest

Cells of the P- and N-starvation cultivations were harvested during late exponential growth phase by vacuum filtration (500 mbar) of aliquots (volume described below) onto polycarbonate filters (Whatman® Nuclepore™ Track-Etched Membranes) with a pore size of 3.0 μm and 0.4 μm for *E. huxleyi* RCC 1216 and RCC 1217, respectively. Cultures for the N-starvation setup were harvested on day 6, for the P-starvation setup *E. huxleyi* RCC 1217 was harvested 1 d before RCC 1216 (day 5 and day 6, respectively). Metabolite analyses via GC-MS required samples of 500 mL culture in total, which were filtered in smaller proportions, to ensure that this process took no longer than 2 min, keeping in mind the high turnover of metabolites. Aliquots of 250 mL were harvested for pigment analyses, and the same volume was used for lipid analyses. The targeted metabolite analyses

via LC-MS/MS only required 20 mL of culture. Filters were immediately frozen in liquid nitrogen and stored at -80°C until further analysis.

Cellular content analysis via FTIR spectroscopy

Cells were cultivated in nutrient-replete ESAW medium as described above. When reaching the late exponential phase at $\sim$$1.4 \times 10^8$ cells in total, they were harvested by filtration, as mentioned above. The cells were removed from the filter with 3 mL 5 M sodium chloride solution (analytical grade, Sigma-Aldrich) and centrifuged at 2500 $\times$ g for 2 min. After removing the supernatant, cells were resuspended in 2 mL of 0.2 M hydrochloric acid (analytical grade, Fisher Chemicals), in order to remove coccoliths (both life-cycle stages were treated analogously). The cells were then directly centrifuged (20,238 $\times$ g, 2 min), and the supernatant was removed. After washing the pellet with 1 mL of the 5 M sodium chloride solution, followed by centrifugation and removal of the supernatant, the resulting pellet was shock frozen in liquid nitrogen and then lyophilized at -55°C and 0.03 mbar (Alpha-14, Christ). FTIR absorption spectra were recorded on an IFS 66/S spectrometer (Bruker) equipped with a photoconductive mercury cadmium telluride (MCT) detector and an attenuated total reflection (ATR) setup (DuraSampl*IR* II, diamond crystal, Smiths) with nine active reflections. The dried biomass was pressed onto the crystal and measured with air as reference. Absorption spectra were collected at a scanning velocity of 150 kHz and a spectral resolution of 2 cm^{-1}. The Fourier transformation was carried out with Mertz phase correction, Blackman-Harris-3-term apodization and a zerofilling factor of 2. For each sample, six measurements were coadded and averaged to a total number of 6144 scans. The spectra were baseline corrected using OPUS 5.5 (Bruker) and normalized to the amide II band at 1539 cm^{-1}. The contribution of alkenes and calcium carbonate to the bands was validated by generating reference spectra of hexatriacontane (98%, Sigma-Aldrich), tetradecane (99%, Acros organics), trans-7-tetradecene (97%, Sigma-Aldrich), and calcium carbonate (>99%, Sigma-Aldrich). Bands of proteins, phospholipids, carbohydrates, and alkenones were identified based on comparison with literature (Giordano et al. 2001; Naumann 2001; Stehfest et al. 2005; Pelusi et al. 2016).

Metabolite analysis via GC-MS

Metabolite extraction, derivatization, and analysis via GC-MS was performed according to Doebbe et al. (2010). 10 μM of ribitol ($\geq$ 99%, Sigma-Aldrich) was used as internal standard. The resulting chromatograms were evaluated with Xcalibur software (Version 2.0.7, Thermo Scientific, Germany). To increase data-confidence, all chromatograms were additionally inspected manually. Metabolites were identified by comparison with previously measured standards and database comparison (NIST 05 library, National Institute of Standards and Technology, Gaithersburg, MD, Thermo Finnigan and the Golm Metabolome Data base (GMD), Max

Planck Institute of Molecular Plant Physiology, Golm, Germany (Kopka et al. 2005)) and reported as "level 1" (identified compound) and "level 2" (putatively identified compound) according to Sumner et al. (2007). Data was normalized to the internal standard and the number of cells present in the sample.

Pigment analysis via UV-VIS-HPLC

Frozen filters were allowed to thaw and all work was carried out in a preferably dark environment. Cells were removed from filter by adding 1 mL of 90% (v/v) acetone (analytical grade), which was saturated with calcium carbonate, to prevent oxidation. The cells were homogenized with 0.1 mm silica beads (Carl Roth) applying three cycles of 45 s at 6500 rpm with 15 s breaks (Precellys 24 homogenizer, Peqlab). After centrifugation at room temperature (5 min, 14,000 rpm), the particle-free supernatant containing pigments was transferred into a HPLC-vial. Samples were coated with N_2 gas and stored at $-20°C$ until analysis. Pigments were separated via HPLC, according to Frommolt et al. (2001). The resulting chromatograms were evaluated with Xcalibur software (Version 2.0.7, Thermo Scientific, Germany). Identification of pigments was based on commercially available pigment standards (DHI group), and peaks were normalized to the number of cells in the sample. The de-epoxidation ratio of the xanthophyll cycle was calculated according to literature (Llewellyn et al. 2007; Ragni et al. 2008), using the equation:

$$\text{De-epoxidation ratio} = \frac{\text{Diatoxanthin}}{(\text{Diatoxanthin} + \text{Diadinoxanthin})} \tag{1}$$

Lipid isolation and separation

Frozen filters were allowed to thaw, then cells were removed from filter by adding 1 mL methanol (HPLC grade) and vortexing. Lipids were isolated using a modified Folch protocol (Bogen et al. 2013) and separated via column chromatography according to Chen et al. (2009). The resulting fractions were further analyzed regarding their fatty acid composition (FAME). The neutral lipid fraction was divided into two parts, of which half was used to analyze FAMEs after derivatization and the other half was used without derivatization to analyze triacylglycerols (TAG), alkenes, and alkenones.

Fatty acid methyl ester (FAME) analysis via GC-MS

Internal standard glycerol triheptadecanoate (1.2 mM, $\geq$ 99%, Sigma-Aldrich) was added to half of the neutral and polar lipid fractions, which were derivatized to gain FAMEs and analyzed via GC-MS as described by Jaeger et al. (2016). The resulting chromatograms were evaluated with Xcalibur software (Version 2.0.7, Thermo Scientific, Germany). Fatty acids were identified and quantified with calibration curves of the Supelco 37 Component FAME Mix (Sigma-Aldrich)

and additional database comparison (NIST 05 library, National Institute of Standards and Technology, Thermo Finnigan).

Triacylglyceride (TAG) analysis via charged aerosol detector (CAD)-HPLC

Part of the remaining half of the neutral lipid fraction was spiked with glycerol triheptadecanoate ($\geq$ 99%, Sigma-Aldrich) as internal standard (1.2 mM) and analyzed via CAD-HPLC, an Ultimate 3000 SD system with dual gradient pump, Accucore C8-column (150 × 4.6 mm, 2.6 μm, Thermo Scientific) and Corona ultra RS detector (Thermo Scientific™ Dionex™ Corona™ ultra RS™ Charged Aerosol Detector), with corona filter set to 4, and 15°C nebulizer temperature. Eluents consisted of methanol : water (65 : 35, v/v) (both LC-MS grade) (A), acetonitrile (LC-MS grade) (B), and isopropanol (GC-MS grade) (C). Flow rates were 0.8 mL min^{-1} for the gradient eluent pump, and 1.2 mL min^{-1} for the inverse gradient pump. The column was heated to 40°C, and the injection volume was 10 μL. Gradients were set as follows; gradient pump: 100% A 10 min before run, 50% A and 50% B at 2 min, 45% A and 55% B at 15 min, 100% B at 23 min, holding until 30 min, then 35% B and 65% C at 60 min. Inverse gradient pump: 66.7% B and 33% C 10 min before run, 33.3% of A, B and C at 2 min, 40% A, 26.7% B and 33.3% C at 15 min, 66.7% A and 33.3% C at 23 min, holding until 30 min, 66.7% A and 33.3% B until 60 min. Resulting peaks were analyzed with the Chromeleon 7.0 software (Thermo Scientific), identified by comparison with commercially available TAG standards (Supelco), and normalized to the internal standard and the number of cells present in sample. To increase data-confidence, all chromatograms were inspected manually.

Alkene analysis via GC-MS

After adding the internal standard hexatriacontane (440 μM, analytical standard grade, Sigma-Aldrich) to the non-derivatized neutral lipid fraction, the samples were analyzed via GC-MS, according to Jaeger et al. (2016). Alkenes were identified by literature comparison (Volkman et al. 1980).

Alkenone analysis via GC-FID

Alkenones were separated from the triacylglycerols and alkenes via column chromatography, using purer silica gel for the chromatography columns (Silica gel 60 extra pure for column chromatography, 0.063-0.200 mm, 70-230 mesh ASTM, Merck). The column was baked for 3 h at 350°C and stored in a desiccator 3 d prior to use. The column was first equilibrated with dichloromethane (GC-MS grade) and then with *n*-hexane (GC-MS grade). The sample was dissolved in *n*-hexane and loaded onto the column. The unwanted lipids were eluted with dichloromethane : *n*-hexane (1 : 1, v/v), after which the alkenone fraction was eluted with dichloromethane. The fractions were evaporated to dryness with nitrogen gas and stored at $-20°C$ until GC-FID analysis.

Alkenone fractions were dissolved in 200 μL *n*-hexane containing the internal standard hexatriacontane (21.1 μM, analytical standard grade, Sigma-Aldrich) and analyzed on a Hewlett Packard gas chromatograph (HP6890, column 30 m $\times$ 0.25 mm; film thickness 0.25 μm; liquid phase: HP 5) using a temperature program as follows: 60°C for 1 min, then increasing to 270°C at 20°C min^{-1}, then to 320°C at 1°C min^{-1}, holding at 320°C for 20 min. A volume of 1 μL was injected (cold injection system: 60°C, 105°C (rate: 3°C s^{-1}), 320°C (rate: 10°C s^{-1}), 320°C (60 s isothermal)). Chromatograms were evaluated with Agilent OpenLab CSD ChemStation Edition for GC systems (Revision C.01.03 (50), Agilent Technologies). Individual alkenone (C$_{37:3}$, C$_{37:2}$) identification was based on retention time and comparison with an external standard. Instrument stability was continuously controlled by reruns of the external alkenone standard during the analytical sequences. The range of the total analytical error calculated by replicate analyses was less than 1%. As a matter of routine several alkenone extracts were saponified in methanolic KOH (ca. 1 mL H$_2$O:MeOH, 1 : 9 v/v; 0.1 M KOH; 120 min, 80°C) to exclude errors by overlapped compounds like C$_{36:3}$ FAME.

Metabolite extraction for amino acid, small organic acid, and osmolyte analysis

For metabolite isolation frozen filters were allowed to thaw, then cells were removed from the filter and suspended in 1 mL 80% (v/v) methanol (LC-MS grade). Cells were disrupted with ultrasonication for 15 min at room temperature. Filters were removed and suspension was centrifuged 10 min at 13,000 $\times$ *g*. The supernatant was used for further analysis.

Amino acid analysis via LC-MS/MS

The analysis of amino acids was conducted by derivatizing dried samples and internal standards (labeled amino acid standards set A, 50 μM, except for glycine: 250 μM, Cambridge Isotope Laboratories) to amino acid butyl esters as described previously (Casetta et al. 2000; Harder et al. 2011). After derivatization, samples were dried again and resolved in 500 μL 0.1% trifluoroacetic acid ($\geq$ 99%, Sigma-Aldrich) in deionized water. Amino acids were separated on a Multospher 120 RP18 AQ-5 μm column (Chromatographie Service). All solvents including water used for LC-MS were LC-MS grade. Eluents consisted of 0.1% trifluoroacetic acid in water (A) and 0.1% trifluoroacetic acid in acetonitrile (B). Flow rate was set to 0.6 mL min^{-1} and 20 μL were injected. The gradient was set as follows: 90% A 15 min before each run, 70% A at 15 min, holding until 19 min, 50% at 26 min, holding until 28 min, 90% A at 30 min. Mass spectrometric analysis (LC-MS/MS) of amino acids was done by using an Agilent 1100 HPLC system (Agilent), connected to an API 4000 quadrupole mass spectrometer (Applied Biosystems/MDS Sciex), which was equipped with an electrospray ionization source, with a mass range of 5-3000 *m/z* at Q1. The individual mass transfers (Q1, Q3) are shown in Supporting

Information Table 1. The resulting chromatograms were evaluated with Analyst software (Version 1.6, AB Sciex). Substances were quantified using external calibration curves of the known standards and normalizing to the recovery of the internal standard. Values were then normalized to the number of cells present in the sample. Performance of the LC-MS/MS was regularly tested using a standard chemical kit (PN 4406127, AB Sciex), containing polypropylene glycol (POS, 2 μM, PN 4405231 and NEG, 30 μM, PN 4405234).

Small organic acid analysis via LC-MS/MS

In order to analyze small organic acids, derivatization was performed in a modified version of a previously published method (Han et al. 2013). 10 μL of succinic acid-d3 as internal standard (Sigma-Aldrich, 5 μg mL^{-1} in methanol) were added to 30 μL of sample. 10 μL of 10% (v/v) pyridine (dried, Merck) in methanol and 50 μL derivatization reagent were added. The derivatization reagent consisted of 50 mM 3-nitrophenylhydrazine (98%, Sigma-Aldrich) in methanol mixed to same parts with 30 mM 1-ethyl-3-(3-dimethylaminopropyl)carbodiimide hydrochloride (EDC, crystalline, Sigma-Aldrich) in methanol. Derivatization was performed for 60 min at 22°C (room temperature). Samples were diluted 1 : 10 in a 1 : 1 mixture (v/v) of methanol and 10 mM ammonium acetate before LC-MS/MS analysis, as described above. The LC-separation was done differently, with a Lichrospher 100 Å RP-C18 EC 125 $\times$ 4 mm, 5 μm column (Merck). Eluent A was methanol and eluent B was 10 mM ammonium acetate in water with a flow rate of 0.5 mL min^{-1} and 30 μL injection volume. The column was equilibrated with 30% A 15 min prior to run. It changed to 80% A after 20 min, holding until 25 min, then went back to 30% after 30 min. Substances were quantified using external calibration curves of known standards and normalizing to the recovery of the internal standard. Values were then normalized to the number of cells present in the sample.

Osmolyte analysis via LC-MS/MS

For the analysis of osmolytes, samples were diluted in acetonitrile : 10 mM ammonium acetate (50 : 50, v/v). Substances were analyzed native via LC-MS/MS, as described in the section above and identified by standards. Again the LC-separation differed, including a Luna NH2 100 Å 250 $\times$ 2 mm, 5 μm LC column (Phenomenex), with a gradient method running with eluent A (acetonitrile) and B (10 mM ammonium acetate) with 0.4 mL min^{-1} flow rate and 20 μL injected sample. The column was equilibrated for 2 min with 80% eluent A prior to each run, then went to 50% A at 1 min, holding until 6 min, returning to 80% eluent A at 7 min, holding until 18 min. The dimethylsulfoniopropionate (DMSP) standard was obtained from Biozol Diagnostica. Dimethylsulfonioacetate, homarine, trimethylammonium propionate and trimethylammonium butyrate standards were synthesized in our laboratory according to Gebser and Pohnert (2013). Validation of synthesized standards was

performed by LC-MS/MS and NMR. Substances were identified by standards and quantified using external calibration curves. Values were then normalized to the number of cells present in the sample.

Polyamine analysis via LC-MS/MS

Samples were derivatized with dansyl chloride in a modified method similar to that of Escribano and Legaz (1988). A mixture of 100 μL sample, 250 μL deionized water, 250 μL saturated sodium bicarbonate solution, and 400 μL 0.02 M dansylchloride ($\geq$ 99%, Fluka) in acetone (HPLC grade) was incubated for 30 min at 60°C. Reaction products were extracted with cyclohexane (99.9%, Merck) and the organic phase was dried. The sample was resolved in 1 mL acetonitrile : water (50 : 50, v/v) with 0.1% acetic acid for LC-MS/MS analysis as described above. The LC separation was different, substances were separated on a Gemini 100 RP-18–3 μ column (Phenomenex) with 0.4 mL min^{-1} flow rate and 20 μL injected sample. Eluents were water with 0.1% acetic acid (A) and acetonitrile (B). The gradient was run as follows: 50% A 15 min before each run, then 10% A at 9 min, holding until 14 min, 50% A at 15 min. Measured standards (all Sigma-Aldrich) included putrescine (99%), cadaverine ($\geq$ 97.0%), spermidine ($\geq$ 99%), and spermine ($\geq$ 99.0%).

Quality controls were performed regularly for LC-MS/MS and GC-FID measurements, in addition to measurements of external standards prior to the measurements. For the GC-MS and HPLC measurements external standards were regularly measured with every run, except for alkenes, which were only identified by literature comparison. Whenever metabolites were quantified, previously assessed calibration curves were used.

Statistical analysis

A two-tailed Student's *t*-test was performed, and statistical significance is indicated by asterisks, representing *p*-values $\leq$ 0.05 (*) and $\leq$ 0.01 (**). All results were shown as mean values or fold-changes of mean values with standard deviation ($\pm$SD). If not stated otherwise, discussed metabolites experienced significant changes above 1.5-fold.

Results

Before in-depth metabolomic analysis of diploid and haploid *E. huxleyi* life-cycle stages and their responses toward nutrient limitation, we investigated the cellular composition of both life-cycle stages under non-limiting conditions.

Cellular composition of the *E. huxleyi* life-cycle stages

Using Fourier transform infrared (FTIR) spectroscopy of whole cell biomass harvested in the exponential growth phase, we were able to compare the cellular composition of the diploid and haploid *E. huxleyi* life-cycle stages (Fig. 1). Cells were acidified to remove coccoliths, which dominated the spectra and interfered with the measurement (Fig. 1a).

Thereafter, characteristic peaks were detected originating mostly from vibrations of proteins (1650 cm^{-1} and 1538 cm^{-1}), phospholipids ($\sim$ 1730 cm^{-1} and 1230 cm^{-1}), and carbohydrates (1200-900 cm^{-1}) (Giordano et al. 2001; Naumann 2001; Stehfest et al. 2005) (Fig. 1b,c). Recently, alkenones in *E. huxleyi* have been semi-quantified using the peak at 963 cm^{-1}, attributed to the *trans*-double bonds (Pelusi et al. 2016). Together with the peak at 1706 cm^{-1} of the keto groups, it is specific for alkenones (Pelusi et al. 2016). Here, the signal at 1706 cm^{-1} could not be isolated, but the contribution of polyunsaturated hydrocarbons, such as alkenones and alkenes, was identified (3013 cm^{-1} and 963 cm^{-1}), being $\sim$10% larger in the diploid (absorbance $A = 0.0046$) (Fig. 1b) than the haploid stage (absorbance $A = 0.042$) (Fig. 1c). Otherwise, the spectra of the diploid and haploid life-cycle stages were highly similar, indicating that no significant differences existed between the cellular composition of both life-cycle stages with respect to proteins, carbohydrates, and lipids.

While there were no differences on this level of analysis, further in-depth metabolomic analysis was applied to acquire a more detailed picture of the biochemical pathways in both life-cycle stages, as well as the influence of nutrient limitation. Two cultivations, including either P- or N-starvation and nutrient-replete controls, were conducted to generate biomass for metabolomic analyses, focusing on general metabolites, proteinogenic amino acids, osmolytes, small carboxylic acids, pigments, and lipids.

Growth of *E. huxleyi* under nutrient starvation

For both cultivation setups, cultures were inoculated with cell densities of $\sim$2000 cells mL^{-1} and grown for 7-8 d, yielding final cell numbers of $\sim$2-3·10^6 cells mL^{-1} for nutrient-replete cultures and of $\sim$1-2·10^6 cells mL^{-1} for nutrient-limited cultures (Fig. 2a,b). In both experimental setups, the nutrient-replete controls of the haploid life-cycle stage reached a higher specific growth rate during the exponential growth phase, compared to the diploid stage (Supporting Information Table 2), the difference being significant for replete cultures of the N-starvation setup (*t*-test, $p = 0.02$). Specific growth obtained over the exponential growth phase did not differ significantly between nutrient-replete and nutrient-starved cultures (Supporting Information Table 2). Samples for metabolite analysis were taken in the late exponential growth phase, as indicated by the arrows. Nutrient analyses of the culture medium up to the metabolome sampling time point confirmed that in the starvation treatments, the limiting nutrients were consumed by day 4, yet not for the replete control cultures (Fig. 2c,d). As the cultures were not aerated to replenish the dissolved inorganic carbon, it was important to monitor total alkalinity, as it can be a limiting factor for calcification of the diploid life-cycle stage. Total alkalinity is decreased by calcification, as precipitation of CaCO$_3$ leads to a decrease of Ca^{2+} concentration,
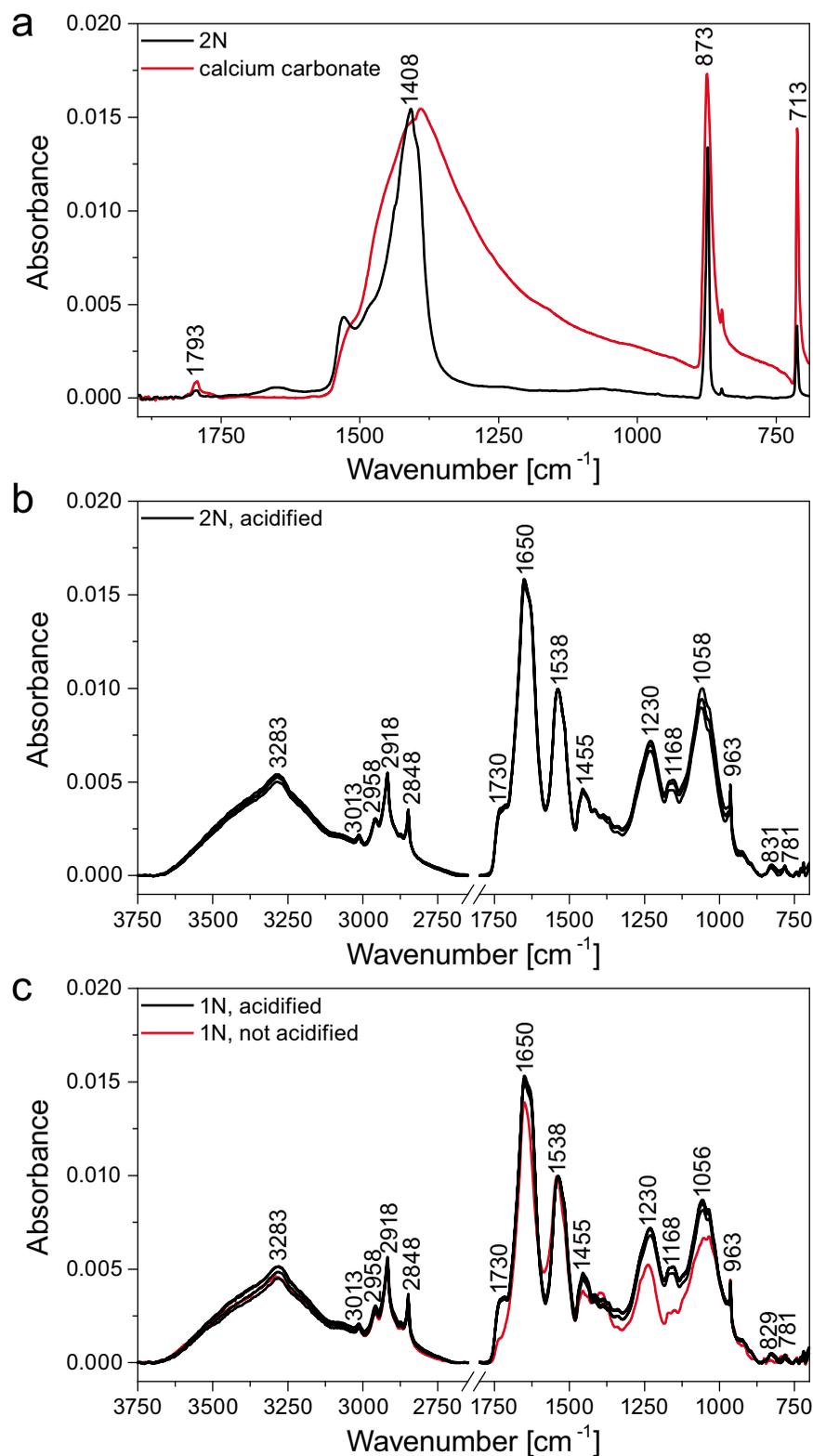
Fig. 1. Fourier transform infrared (FTIR) spectra of diploid (2N) and haploid (1N) *E. huxleyi* life-cycle stages, showing little difference in cellular content. (**a**) The spectrum of the 2N life-cycle stage (black line) contains dominant signals at 1408 cm^{-1} and 873 cm^{-1}, assigned to calcium carbonate (red line) of the coccoliths, which interfere with the measurement. (**b**) Spectra of four biological replicates of the 2N life-cycle stage after acidification to remove the coccoliths. (**c**) Spectra of four biological replicates (black lines) of the 1N life-cycle stage after acidification. Acidification had little effect on the 1N life-cycle stage (red line). Deviations at 1730 cm^{-1} and around 1200 cm^{-1} are a consequence of the change in pH. Lyophilized biomass was harvested in the late exponential growth phase. Mean values of six technical measurements are denoted. Assignment of the peaks: 3700-3100 cm^{-1} and 3000-2800 cm^{-1}: unspecific region originating from O-H, N-H and C-H stretching vibrations; ~1730 cm^{-1}: C=O-vibrations of ester groups, primarily of phospholipids; 1650 cm^{-1} and 1538 cm^{-1}: amide I and amide II bands of proteins; 1470-1350 cm^{-1}: unspecific region originating from C-H bending vibrations; 1230 cm^{-1} and ~1085 cm^{-1}: contributions from phosphodiester vibrations of phospholipids, among others; 1200-900 cm^{-1}: coupled stretching and bending vibrations associated with carbohydrates; 3013 cm^{-1} and 963 cm^{-1}: =C-H stretching modes and hydrogen-out-of-plane modes of *trans*-double bonds of unsaturated hydrocarbons such as alkenones.
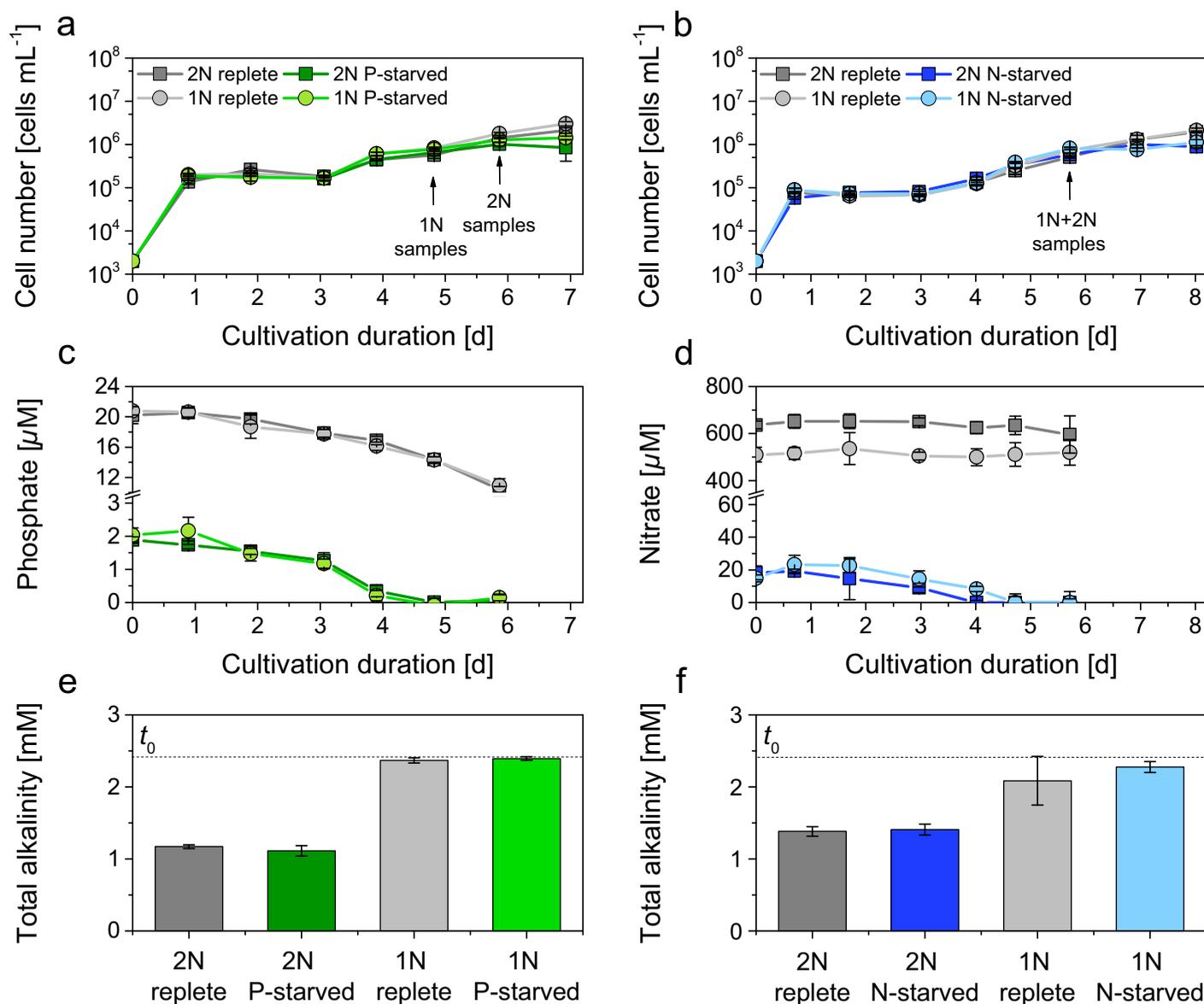
Fig. 2. Growth characteristics for *E. huxleyi*. (**a**) Cell numbers for the P-starvation setup with 2N (boxes) and 1N (circles), in nutrient-replete (gray) and P-limited ESAW medium (green), arrows indicate metabolome sampling time points. (**b**) Cell numbers for the N-starvation setup with 2N (boxes) and 1N (circles), in nutrient-replete (gray) and N-limited ESAW medium (blue), arrows indicate metabolome sampling time points. (**c**) Phosphate concentration in the medium for the P-starvation setup. (**d**) Nitrate concentration in the medium for the N-starvation setup. (**e**) Total alkalinity at the metabolome sampling time points, 2N and 1N under nutrient-replete (gray) and P-starved conditions (green). (**f**) Total alkalinity at the metabolome sampling time point, 2N and 1N under nutrient-replete (gray) and N-starved conditions (blue). The dotted line indicates the total alkalinity at the start of the cultivation (t_0). Mean values of three biological replicates with triplicate measurements ($n = 3$) are denoted, error bars represent standard deviations (SD).

resulting in a decrease of charge differences between conservative cations and anions (Zeebe and Wolf-Gladrow 2001). Total alkalinity at the metabolome sampling time point was indeed lower in all diploid cultures due to calcification, reaching minimal values of ~1.17 mM (Fig. 2e,f). However, there was no difference between replete- and nutrient-limited cultures, confirming that the only limitation stems from nutrient depletion.

Metabolite analysis

In order to analyze the effect of nutrient starvation on the metabolome of the diploid and haploid life-cycle stages of *E. huxleyi*, we applied ten different specific metabolome analysis methods. For example, GC-MS measurements allowed the identification of general primary metabolites. The application of LC-MS/MS allowed more specific metabolome analyses, with four different derivatization and

separation methods, enabling the quantification of free amino acids, small carboxylic acids, osmolytes, and amines. Photosynthetic pigments were detected via UV-VIS-HPLC analysis. Additionally, we applied four different lipid analysis methods, allowing identification of fatty acids belonging to neutral and polar lipids (GC-MS), neutral lipid triacylglycerols (TAGs) (CAD-HPLC), alkenes in the neutral lipid fraction (GC-MS), and neutral lipid alkenones (GC-FID).

In more detail, GC-MS measurements were conducted after derivatization of the metabolite extract with N-Methyl-N-(trimethylsilyl)trifluoroacetamide (MSTFA), allowing the identification of primary metabolites. Further metabolites were detected after substance-specific derivatization and separation via LC-MS/MS, such as three different osmolytes (dimethylsulfoniopropionate (DMSP), glycine betaine and homarine), six small carboxylic acids (α-ketoglutarate, citrate, lactate, malate, pyruvate, succinate), as well as 19 of the canonic proteinogenic amino acids. Unfortunately, we were not able to detect any amines in *E. huxleyi*, as concentrations were below the detection limit. The same is true for the osmolytes dimethylsulfonioacetate, trimethylammonium propionate and trimethylammonium butyrate. Measurements of acetone extracts via UV-VIS-HPLC led to the identification of ten different photosynthetic pigments, all typical for *E. huxleyi* (Stolte et al. 2000). The applied lipid-detection method via fatty acid methyl ester (FAME) derivatization allowed elucidation of the fatty acid chain length from diverse polar lipids (i.e., membrane compounds, diglycerides, sphingolipids) as well as the chain lengths from neutral lipids (i.e., TAGs, wax esters, sterols, and free fatty acids). *E. huxleyi*'s polar lipid fraction contained 12 different fatty acid chain lengths, including some that were absent in the neutral fraction, such as odd-numbered $C_{15:0}$, which have been reported before (Pond and Harris 1996; Riebesell et al. 2000), and additional unsaturated compounds ($C_{18:1n9tr}$, $C_{18:4n3}$, $C_{22:1n9}$). Eight different fatty acid chain lengths were detected in *E. huxleyi*'s neutral lipid fraction.

To get a more detailed insight into the composition of storage lipids in the neutral lipid fraction, we specifically measured whole TAGs from the non-derivatized neutral lipid fraction via CAD-HPLC. In *E. huxleyi*, TAGs only represent a small fraction of the neutral lipids (Volkman et al. 1986; Bell and Pond 1996; Malitsky et al. 2016). Five TAGs could be identified based on comparison with commercially available standards that were comprised of identical chain lengths (e.g., three $C_{14:0}$ chains attached to one glycerol backbone). However, the majority of TAGs (15 compounds) was composed of odd-numbered chain lengths, which could not be further identified, due to unavailability of suitable standards. It is, however, not likely that these are mono- or diacylglycerols, as these are not present in the neutral lipid fraction. Additionally, such compounds, by experience, generally elute earlier from the column (retention time 18-20 min, compared to first TAG $C_{8:0}$, 21 min).

Furthermore, a big proportion of *E. huxleyi*'s neutral lipid fraction consists of polyunsaturated long-chain alkenes and alkenones (Volkman et al. 1980; Sawada et al. 1996; Eltgroth et al. 2005). The analysis of the non-derivatized neutral lipid fraction via GC-MS led to the identification of two isomers of a $C_{31:2}$ alkene. Further purification of this fraction led to the detection of six polyunsaturated methyl (Me) and ethyl (Et) alkenones via GC-FID, namely $C_{37:2}$ Me, $C_{37:3}$ Me, $C_{38:2}$ Me, $C_{38:2}$ Et, $C_{38:3}$ Me, and $C_{38:3}$ Et. From these C_{37} alkenone data the $U^{K'}_{37}$ paleothermometry proxy can be derived (Conte et al. 1998). For more details on the paleothermometry, which was not the focus of this study, we refer to Supporting Information 1.

In the following section, the metabolic patterns of both life-cycle stages and their peculiarities under nutrient-replete conditions are compared first, to identify possible general metabolome features, and also to find representative patterns that are exclusive for the two ploidy stages. Subsequently, the metabolic responses of both life-cycle stages to phosphorus starvation are elaborated, and commonalities and peculiarities of the respective responses are evaluated and correlated with previously obtained transcriptomic and other data. Last, the individual responses of both life-cycle stages to nitrogen starvation are assessed and evaluated alike.

Metabolomes of non-limited life-cycle stages

The nutrient-replete samples of both cultivation setups (Fig. 2a,b) were used to elucidate differences of the metabolite levels between the diploid and the haploid *E. huxleyi* life-cycle stages. These differences were then quantified and are shown as a heat map in Fig. 3a. All absolute data can be found in Supporting Information Table 3 and online at https://doi.org/10.1594/PANGAEA.876214.

The comparison of both life-cycle stages under nutrient-replete conditions revealed significant differences in the metabolite profiles. In the diplont, compared to the haplont, increased metabolite abundances were found for 66 out of 105 detected metabolites. While 45 metabolites were at least 1.5-fold increased, the change was statistically significant for 35 of these metabolites. If not stated otherwise, metabolites discussed throughout the text experienced statistically significant changes above 1.5-fold. The diploid stage contained a higher abundance of certain amino acids (glutamate, homoserine, lysine, threonine, valine), nucleotides (adenine), sugars (melibiose), osmolytes (DMSP), photosynthetic pigments (19′-hexanoyloxy-4-ketofucoxanthin), TAGs (TAG $C_{8:0}$, 12 unknown TAGs), alkenes (two isomers of $C_{31:2}$ alkene), alkenones ($C_{37:2}$ Me, $C_{37:3}$ Me, $C_{38:2}$ Me, $C_{38:2}$ Et, $C_{38:3}$ Me), neutral lipid associated fatty acids ($C_{14:0}$), and polar lipid associated fatty acids ($C_{18:1n9cis}$, $C_{18:2n6cis}$, $C_{18:4n3}$, $C_{22:0}$, $C_{22:6n3}$).

In contrast to other metabolites, the concentration of the osmolyte DMSP varied considerably between nutrient-replete controls of the separate cultivation setups (Supporting
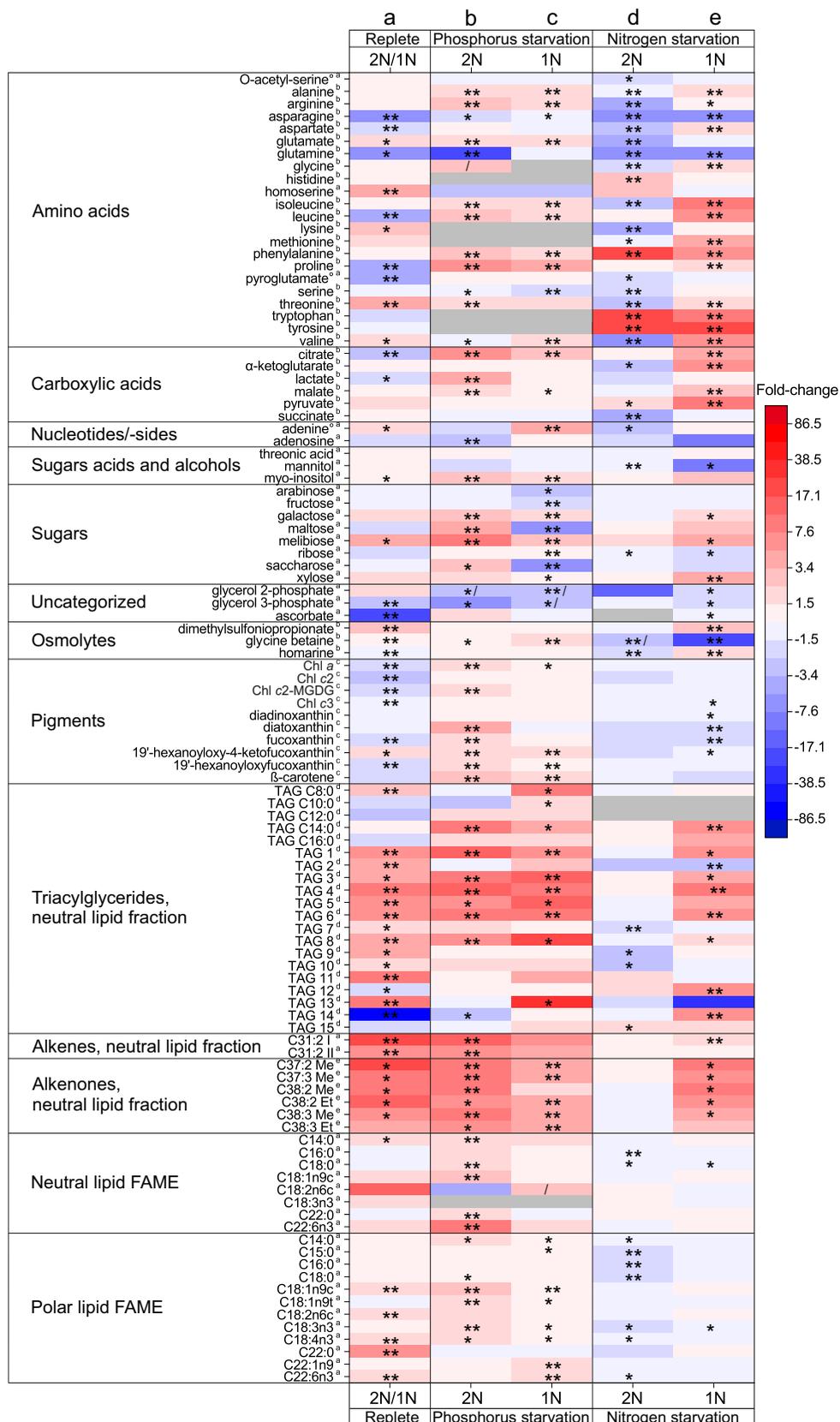
Fig. 3. Heat map of the fold-changes of increased (red) or decreased (blue) metabolites for *E. huxleyi* 2N and 1N under macronutrient starvation. (**a**) Comparison of metabolite abundance between nutrient-replete 2N and 1N life-cycle stages, over both cultivation setups. (**b**, **c**) Fold-changes of metabolite abundance for P-starved 2N (**b**) and 1N (**c**) life-cycle stages compared to the respective nutrient-replete control. (**d**, **e**) Fold-changes of metabolite abundance for N-starved 2N (**d**) and 1N (**e**) cells compared to their respective replete control. Gray boxes indicate that the metabolite was not detected. Metabolites that were detected in one treatment but not in the other were marked with /, indicating manually added tendency of fold-change (calculation of fold-change inaccurate, due to division by zero). Asterisks represent *p*-values as determined via Student's *t*-test (* represents *p*-values ≤ 0.05, ** represents *p*-values ≤ 0.01). Letters denote the instrument used to detect the metabolite ([a]GC-MS, [b]LC-MS/MS, [c]UV-VIS-HPLC, [d]CAD-HPLC, [e]GC-FID). Metabolites marked with ° were identified by data base comparison of *m/z* values (level 2, putatively identified compound), all other metabolites were additionally confirmed by measured standards (level 1, identified compound). Values represent fold-changes of mean values of six (**a**, *n* = 6) or three (**b**–**e**, *n* = 3) biological replicates measured in technical duplicates/triplicates. All absolute data can be found in Supporting Information Table 3. c, cis; FAME, fatty acid methyl ester; MGDG, monogalactosyldiacylglycerol; t, trans; TAG, triacylglycerol.

Information Table 3), as indicated by the high standard deviation of the pooled replete replicates (2N replete: 491 ± 198 fg cell^{-1}, 1N replete: 218 ± 110 fg cell^{-1}). In the nutrient-replete controls of the P-starvation setup, diploid cells contained 11.5-fold more DMSP than the haploid cells (304 ± 23 fg cell^{-1} vs. 32 ± 12 fg cell^{-1}, respectively). In the nutrient-replete controls of the N-starvation cultivation, the DMSP concentration was 1.7-fold higher in the diploid cells than in the haploid cells, but generally with significantly higher amounts (678 ± 88 fg cell^{-1} vs. 402 ± 65 fg cell^{-1}, respectively).

Furthermore, 39 metabolites were found in lower abundance in the diploid life-cycle stage compared to the haploid stage. A decrease of at least 1.5-fold was found for 26 of these metabolites, with a significant change for 17 of these. These included amino acids (asparagine, aspartate, glutamine, leucine, proline, pyroglutamate), carboxylic acids (citrate, lactate), phosphoric esters (glycerol 3-phosphate), vitamins (ascorbate), photosynthetic pigments (Chl a, Chl c_2, Chl c_2-MGDG, fucoxanthin, 19′-hexanoyloxyfucoxanthin), and TAGs (two unknown TAGs).

The effect of P-starvation on *E. huxleyi* life-cycle stages

In order to analyze the effect of P-starvation on *E. huxleyi*, fold-change values were calculated for the metabolite abundances of the P-starved cultures in comparison to the respective nutrient-replete controls. As a general tendency in both life-cycle stages, the majority of all detected metabolites were increased under P-starvation compared to nutrient-replete conditions (Fig. 3b,c, absolute data in Supporting Information Table 3).

In the diploid life-cycle stage 77 out of 105 detected metabolites were increased under P-starvation (Fig. 3b). An increase of at least 1.5-fold was found for 56 of these metabolites, 48 of which changed significantly. These included amino acids (alanine, arginine, glutamate, isoleucine, leucine, phenylalanine, proline, threonine), carboxylic acids (citrate, lactate, malate), sugar alcohols (myo-inositol), sugars (galactose, maltose, melibiose, saccharose), photosynthetic and photoprotective pigments (Chl a, Chl c_2-monogalactosyldiacylglycerol (MGDG), diatoxanthin, fucoxanthin, 19′-hexanoyloxy-4-ketofucoxanthin, 19′-hexanoyloxyfucoxanthin, β-carotene), TAG (TAG $C_{14:0}$, six unknown TAG), alkenes (two isomers of $C_{31:2}$ alkene), alkenones ($C_{37:2}$ Me, $C_{37:3}$ Me, $C_{38:2}$ Me, $C_{38:2}$ Et, $C_{38:3}$ Me, $C_{38:3}$ Et), neutral lipid associated fatty acids ($C_{14:0}$, $C_{18:0}$, $C_{18:1n9cis}$, $C_{22:0}$, $C_{22:6n3}$), and polar lipid associated fatty acids ($C_{14:0}$, $C_{18:1n9cis}$, $C_{18:1n9tr}$, $C_{18:3n3}$, and $C_{18:4n3}$). The amino acid glycine was technically also increased compared to replete conditions, as it was only detected under P-starvation. Contrasting to the high number of increased metabolites, only 22 out of 105 metabolites were decreased in abundance. Ten of these were decreased at least 1.5-fold, five of which were significantly changed. These included amino acids (asparagine,

glutamine), nucleosides (adenosine), phosphate esters (glycerol 3-phosphate), and TAG (one unknown TAG). Technically, glycerol 2-phosphate was also decreased compared to replete conditions, as it was not detected under P-starvation.

In the haploid life-cycle stage, a similar pattern was observed under P-starvation (Fig. 3c), involving an increase of 79 out of 105 metabolites. A threshold of 1.5-fold was reached for 45 metabolites, of which 33 were changed significantly. These included amino acids (alanine, arginine, glutamate, isoleucine, leucine, phenylalanine, proline, valine), carboxylic acids (citrate), nucleotides (adenine), sugar alcohols (myo-inositol), sugars (galactose, melibiose), osmolytes (glycine betaine), photosynthetic and photoprotective pigments (19′-hexanoyloxy-4-ketofucoxanthin, β-carotene), TAGs (TAG $C_{8:0}$, TAG $C_{10:0}$, TAG $C_{14:0}$, seven unknown TAGs), alkenones ($C_{37:2}$ Me, $C_{37:3}$ Me, $C_{38:2}$ Et, $C_{38:3}$ Me, $C_{38:3}$ Et), and polar lipid associated fatty acids ($C_{22:1n9}$ and $C_{22:6n3}$). Similar to the results of the diploid life-cycle stage, few metabolites were decreased in the haplont. Nineteen out of 105 metabolites decreased, six being decreased more than 1.5-fold, five of which changed significantly. These included amino acids (serine) and sugars (arabinose, fructose, maltose, saccharose). Technically, glycerol 2-phosphate and glycerol 3-phosphate also decreased under P-starvation, as they were not detected under these conditions.

The effect of N-starvation on *E. huxleyi* life-cycle stages

To analyze the effect of N-starvation on *E. huxleyi*, again fold-changes were calculated for the metabolites of the starved cultures in comparison to the respective nutrient-replete controls of the N-starvation setup (Fig. 3d,e, absolute data in Supporting Information Table 3). In contrast to the previously observed general increase of metabolite abundances under P-starvation, N-starvation led to an overall decrease of metabolite abundance, at least for most metabolites detected in the diploid life-cycle stage (Fig. 3d).

In the diploid stage, only 27 out of 105 detected metabolites were increased. Ten metabolites were increased more than 1.5-fold, six of which were changed significantly. These included amino acids (histidine, phenylalanine, tryptophan, tyrosine), carboxylic acids (pyruvate), and TAGs (one unknown TAG). Contrastingly, 75 out of 105 metabolites were decreased in the diploid stage under N-starvation. A decrease of at least 1.5-fold was reached by 34 metabolites, of which 24 were significantly changed. These included amino acids (O-acetyl-serine, arginine, asparagine, aspartate, glutamate, glutamine, glycine, isoleucine, lysine, pyroglutamate, serine, threonine, valine), carboxylic acids (α-ketoglutarate, succinate), nucleotides (adenine), osmolytes (homarine), TAG (three unknown TAGs), and polar lipid associated fatty acids ($C_{15:0}$, $C_{16:0}$, $C_{18:0}$, and $C_{18:3n3}$). The osmolyte glycine betaine technically also decreased, as it was not detected under N-starvation in the diploid stage.

In the haploid stage, metabolite abundances under N-starvation did not follow the mentioned general decrease observed in the diploid stage, except for pigments (Fig. 3e). Instead, many metabolites in the haplont were increased in abundance, as previously observed for both stages under P-starvation. In more detail, increased abundances were found for 58 out of 105 detected metabolites, 41 being at least 1.5-fold increased, of which 35 were significantly changed. These included amino acids (alanine, aspartate, glycine, iso-leucine, leucine, methionine, phenylalanine, proline, threo-nine, tryptophan, tyrosine, valine), carboxylic acids (citrate, α-ketoglutarate, malate, pyruvate), sugars (galactose, meli-biose, xylose), osmolytes (DMSP, homarine), TAGs (TAG $C_{14:0}$, seven unknown TAGs), alkenes (one isomer of the $C_{31:2}$), and alkenones ($C_{37:2}$ Me, $C_{37:3}$ Me, $C_{38:2}$ Me, $C_{38:2}$ Et, $C_{38:3}$ Me). Decreased abundances were detected for 45 out of 105 metabolites under N-starvation. The decrease was at least 1.5-fold for 14 metabolites, of which 10 changed signif-icantly. Among these were amino acids (asparagine, gluta-mine), sugar acids (mannitol), sugars (ribose), phosphate esters (glycerol 2-phosphate, glycerol 3-phosphate), osmo-lytes (glycine betaine), photosynthetic and photoprotective pigments (diatoxanthin, fucoxanthin), and TAGs (one unknown TAG).

Discussion

The aim of this work was to analyze the effect of P- and N-starvation on the intracellular metabolome of diploid and haploid *E. huxleyi* life-cycle stages. As P- and N-limitation are very common in the ocean, this dataset facilitates the under-standing of how the different life-cycle stages cope with nutrient starvation. We applied several different metabolo-mic analysis methods to obtain a picture of the intracellular metabolome, covering a large number of different metabolites.

The lowered total alkalinity observed in the cultures of the diploid stage results from the uptake of calcium ions for calcification (Zeebe and Wolf-Gladrow 2001). Although we cannot fully rule out that shifts in total alkalinity affect the metabolome, such effects are highly unlikely, because total alkalinity is a chemical, somewhat artificial parameter that cannot per se be sensed by microorganisms. If at all, rather the drifting speciation of dissolved inorganic carbon species toward higher CO_2 concentrations may have affected the instantaneous carbon uptake (Kottmeier et al. 2016). Neither the inorganic carbon species, nor the ions that constitute total alkalinity were drawn down to limiting concentrations. Apart from this, such shifts in the carbonate system are unavoidable in bloom-experiments and were also obtained in the previous transcriptome studies by Rokitta et al. (2014, 2016). Thus, these shifts in the carbonate system do not hamper the comparison of data within and across studies.

Life-cycle stages have distinct metabolite patterns

Under nutrient-replete conditions, there was a noticeable difference in the metabolic profile of the diploid and haploid life-cycle stages, with 46 out of 105 metabolites showing a significant difference of at least $\pm$ 1.5-fold (Fig. 3a). The main differences were the higher content of DMSP and TAGs in the diploid stage.

DMSP, an osmolyte with cryoprotective and antioxidative properties (Sunda et al. 2002), was the most abundant osmo-lyte in the whole dataset (Supporting Information Table 3), in line with previous findings (Gebser and Pohnert 2013). Our data show high variability of DMSP contents in the sep-arate nutrient-replete setups. Comparison of various studies also reveals general differences in the DMSP concentration, showing that separate cultivations cannot necessarily be directly compared (Gebser and Pohnert 2013). The more pro-nounced difference for nutrient-replete stages of the P-starvation setup could derive from the difference in harvest-ing time point, which has been reported before (Keller et al. 1999). We also found a significantly higher concentration of DMSP in the diploid stage, as has been shown before for the exact same *E. huxleyi* life-cycle stages (2N: 580 fg cell^{-1} vs. 1N: 380 fg cell^{-1}) (Spielmeyer et al. 2011). Osmolyte abun-dance is influenced by salinity (Gebser and Pohnert 2013), however we assume that salinity (calculated as 31.27 g kg^{-1}) did not change during cultivation. It is more likely that the lower DMSP abundance in the haploid stage is caused by an increased turnover of DMSP to dimethylsulfide (DMS), reported at transcriptomic level for DMSP lyase (Rokitta et al. 2011, Alcolombri et al. 2015), which catalyzes the reac-tion. The different DMSP abundance could also be explained by differences in antioxidant composition (Stefels 2000). It remains to be studied whether the high abundance of DMSP has any negative side effect on the diploid cells in terms of osmolytic homeostasis, redox-control or maintenance of cel-lular compartmentation. So far, the mode of action of this molecule remains unknown (Sunda et al. 2002; Georg Poh-nert pers. comm.). The generally higher concentration of DMSP in the diploid life-cycle stage could indicate, in a first approximation, a higher need to maintain osmotic balance. The need for stronger osmoregulation in this stage could be connected to the process of calcification, in which large amounts of Ca^{2+} and HCO_3^- are imported into the coccolith forming endomembraneous apparatus. The occurring pre-concentration of Ca^{2+} ions in a vacuole-like compartment (Sviben et al. 2016) could possibly require such a strong intracellular osmoregulation. Similarly argued, the additional endomembraneous structures required for pre-concentration and the precipitation of calcium carbonate inside the cells may also be the reason for the significantly higher lipid abundances compared to the non-calcifying haploid stage.

Further metabolites with osmolytic properties were man-nitol and proline. Mannitol, a sugar alcohol with osmopro-tective properties, was found to be one of the most

abundant metabolites throughout the dataset (Supporting Information Table 3), which is in line with previous findings (Obata et al. 2013; Mausz and Pohnert 2015). It also functions as a carbon and reductant storage in *E. huxleyi* (Obata et al. 2013; Tsuji et al. 2015). In the pooled replicates, there was no significant difference in mannitol abundance between the life-cycle stages (Fig. 3a). Focusing on the separate cultivations (Supporting Information Table 3), mannitol abundance was similar for both life-cycle stages in the nutrient-replete controls of the N-starvation setup. It was comparably lower in the nutrient-replete controls of the P-starvation setup, however, where the diploid stage also contained 2.6-fold more mannitol compared to the haploid stage, indicating differences in carbon storage and possibly osmolarity. The proline concentration was significantly higher in the haploid stage in this study, possibly to balance osmotic pressure. However, as these osmolytes also have other functions, this is difficult to interpret.

Under nutrient-replete conditions, the haploid stage contained more citrate, as previously reported (Mausz and Pohnert 2015), as well as more lactate. At the same time, it contained less succinate compared to the diploid stage. This could be partially explained by the prominent up-regulation of the carboxylic acid and energy metabolism in the haploid stage, which was previously observed at the transcriptomic level (Rokitta et al. 2011). It was hypothesized that the haploid life-cycle stage requires relatively more energy to fuel its flagellar apparatus to facilitate motility (Rokitta et al. 2011), explaining increased activity of the tricarboxylic acid cycle.

With respect to pigment composition, there were prominent differences between the life-cycle stages. Compared to the haploid stage, the diploid stage contained a significantly higher amount of 19′-hexanoyloxy-4-ketofucoxanthin, as well as a significantly lower amount of Chl *a*, Chl c_2, Chl c_2-MGDG, and the carotenoids fucoxanthin and 19′-hexanoyloxyfucoxanthin, which may suggest different photosynthetic capabilities between the life-cycle stages. No significant differences in pigment abundance between both life-cycle stages were reported in a previous study, even though the diploid stage showed a lower chlorophyll-based photosynthetic performance than the haploid stage grown at comparable irradiances (Houdan et al. 2005). These results do, however, not agree a different publication, where the diploid stage showed a slightly higher chlorophyll-normalized performance in net photosynthesis than the haploid stage under nutrient-replete conditions (Rokitta and Rost 2012). Based on photoinhibition, observed in the haploid stage at much lower irradiances than the diploid stage, differences in niche separation have been hypothesized for these life-cycle stages (Houdan et al. 2005).

Noticeable differences were also observed in the abundances of TAGs, which only represent a comparably small fraction of the total neutral lipids in *E. huxleyi* (Volkman et al. 1986; Bell and Pond 1996; Malitsky et al. 2016). We found various medium-chained TAGs ($C_{8:0}$-$C_{12:0}$), which might be well exploitable as biofuel components (Knothe et al. 2009). So far, TAG in *E. huxleyi* has only been reported as total TAG (Volkman et al. 1986; Bell and Pond 1996; Pond and Harris 1996; Rosenwasser et al. 2014), or as the sum of all three fatty acids for TAG (Malitsky et al. 2016), complicating comparison with our data. The diploid life-cycle stage contained a 2.9-fold higher total cellular amount of TAGs under nutrient-replete conditions than the haploid stage (Supporting Information Table 3), indicating a generally higher capability to store energy in form of TAGs. This also correlates with the postulated higher respiratory activity of the haploid stage, which is thought to make intense use of fatty compounds to fuel mitochondrial energy generation in order to drive flagellar movement (Rokitta et al. 2011).

The higher amount of alkenones in the diploid *E. huxleyi* life-cycle stage confirms the results obtained via FTIR (Fig. 1), and is in line with Bell and Pond (1996). This could be connected to buoyancy regulation (Fernández et al. 1994) or coccolith vesicle structure (Sawada and Shiraiwa 2004), although the presence of alkenones in coccolith vesicles is still under debate (Eltgroth et al. 2005).

The detected polar lipid fatty acids are components of polar lipids of *E. huxleyi* (Bell and Pond 1996; Fulton et al. 2014). We did not detect $C_{18:5}$, in line with Fiorini et al. (2010), who did not detect it in the same diploid stage and found only traces in the haploid stage. This apparent discrepancy could be attributed to cultivation temperature and thus membrane fluidity (van Wagenen et al. 2012), as our and Fiorini's work was conducted at 20°C and 19°C, respectively, whereas studies detecting $C_{18:5}$ were performed at 15°C (Volkman et al. 1981; Bell and Pond 1996; Pond and Harris 1996; Dijkman and Kromkamp 2006; Evans et al. 2009). The occurrence of three Ω-3 fatty acids ($C_{22:6n3}$, $C_{18:3n3}$, and $C_{18:4n3}$) make this alga important for aquacultural feed (Bell and Pond 1996; Sayanova et al. 2011). The presence of these Ω-3 fatty acids in polar as well as neutral lipids is unusual for microalgae (Martins et al. 2013), and could simplify extraction processes for upscaled industrial use. Also, an odd-numbered fatty acid ($C_{15:0}$) was found in the polar FAME fraction, which has been reported before in different *E. huxleyi* strains (Pond and Harris 1996; Riebesell et al. 2000), but is still uncommon among microalgae.

The diploid *E. huxleyi* stage also had a slightly higher concentration of polar lipids under nutrient-replete conditions, especially concerning the fatty acids $C_{18:1n9cis}$, $C_{18:2n6cis}$, $C_{18:4n3}$, $C_{22:0}$, and $C_{22:6n3}$, indicating differences in membrane composition. The higher abundance of polyunsaturated fatty acids could reflect differences in thylakoid membrane composition (Fulton et al. 2014), which has been shown for haploid and diploid *E. huxleyi* strains before (Bell and Pond 1996; Fiorini et al. 2010; Hunter et al. 2015), and could influence photosynthetic efficiency (Kobayashi et al. 2016). As mentioned above, differences in polar lipid

composition could be attributed to diploid-specific compartments such as vesicles for calcium carbonate pre-concentration (Sviben et al. 2016), and coccolith vesicle structures (Sawada and Shiraiwa 2004; Eltgroth et al. 2005), or viral susceptibility (Hunter et al. 2015).

P-starvation boosts metabolite contents in both life-cycle stages

In the P-starvation setup, there was a 24 h offset regarding the metabolite sampling time of the life-cycle stages. However, at both time points, the respective nutrient in the culture medium was limited and the metabolic rearrangements clearly show that P-starvation had an effect. Further, it can be interpreted from transcriptomic, time-resolved data on starvation scenarios that cellular responses toward P-starvation are triggered by the cell in an "all or nothing" manner, so that early and late P-starvation responses differ not qualitatively but quantitatively (Rokitta et al. 2016).

For comparison of the metabolome data gathered in this work, and the transcriptome data from a different cultivation (Rokitta et al. 2014, 2016), it is necessary to address differences between the cultivations. In contrast to the earlier transcriptome study, slightly higher light intensity and temperature prevailing in our lab led to faster cell growth, which is why cells were harvested somewhat earlier compared to the previous work. As nutrient depletion was reached prior to harvest for cells grown in nutrient deplete medium (Fig. 2c,d), and cell numbers dropped during further cultivation of remaining culture volume (Fig. 2a,b), this indicates that the stage of nutrient starvation was just before cell death, therefore late starvation, and thus comparable with the transcriptome harvest.

For both life-cycle stages, P-starvation resulted in a significant accumulation of several key metabolites, indicating that cells experience a "metabolic overflow": Several amino acids were increased under P-starvation in both stages, which correlates with the shutdown of cell cycling and protein synthesis as indicated by the correlating transcriptomic data (Rokitta et al. 2016). This is also in line with decreased protein abundance observed previously under P-starvation in *E. huxleyi* (McKew et al. 2015) and in other microalgae (Zhao et al. 2009).

A significant increase of proline was observed in both stages under P-starvation, supporting the hypothesis that proline and its mitochondrial oxidation play a central regulatory role in arresting the cell cycle under starvation, possibly by inducing mitochondrial oxidative stress and related signaling (Phang et al. 2012; Rokitta et al. 2016).

Like in the nutrient-replete treatments, the most abundant osmolyte under P-starvation was DMSP (Supporting Information Table 3), suggesting that, in the diploid life-cycle stage, it is continuously produced during P-starvation, in line with Wilson et al. (1998). Furthermore, glycine betaine was significantly increased in both life-cycle stages in

this study. It can be assumed that betaine osmolytes, such as glycine betaine and homarine, are further used for betaine lipids to replace phospholipids, which is known to occur in *E. huxleyi* and other marine microalgae under P-starvation (van Mooy et al. 2009; Shemi et al. 2016).

Lactate content (D and/or L) was generally high and further increased under P-starvation in both life-cycle stages, although insignificantly in the haploid stage. This observation advocates the hypothesis brought up by Rokitta et al. (2016) that the methylglyoxal pathway, with L-lactate as an intermediate, is prominently up-regulated in starvation situations and during cell-cycle arrest. Besides giving rise to the cytostatic compound methylglyoxal, this pathway constitutes an alternative way to synthesize cytoplasmic ATP despite disturbed glycolytic flux (Inoue et al. 1985; Chakraborty et al. 2014). However, flux-balance analyses would be necessary to ultimately prove an up-regulation of this pathway, as there is no consensus that intermediate accumulation necessarily indicates up-regulation. Nonetheless, activation of the glycolytic bypass under P-starvation has been hypothesized for other microalgae (Theodorou et al. 1991; Wurch et al. 2011; Dyhrman et al. 2012).

Beyond lactate, P-starvation resulted in roughly a doubling of the cellular contents of small carboxylic acids in both life-cycle stages, among them metabolites of the tricarboxylic acid cycle, e.g., citrate, and malate. Since transcriptomic data showed a down-regulation of enzymes involved in the respiratory electron-transfer chain (Rokitta et al. 2016), it is likely that the compounds indeed accumulate due to a general decrease of mitochondrial respiratory activity. Transcriptomic data also indicated an up-regulation of malate-quinone-oxidoreductase under P-starvation in both life-cycle stages, indicating re-routed electron input to the respiratory chain via this enzyme (Rokitta et al. 2016), in line with the higher malate abundance observed in this study. Transcripts of enzymes for lipid turnover and traffic were also increased, indicating increased lipid turnover and flux across the mitochondrial malate/citrate mechanism (Rokitta et al. 2016). This could further explain the increased citrate abundances observed in this study, as citrate can be converted to acetyl-CoA, which is used for de-novo fatty acid synthesis (Bellou and Aggelis 2012).

A prominent increase of several chlorophylls and carotenoids was detected under P-starvation in the diploid stage, confirming previously published results obtained under P-starvation for *E. huxleyi* (McKew et al. 2015) and other microalgae (Kozlowska-Szerenos et al. 2004). In the haploid stage, several pigments were also increased, although only few were increased significantly above 1.5-fold. Interestingly, the de-epoxidation ratio of the xanthophyll cycle (Eq. 1) increased significantly in the diploid stage under P-starvation in this study (Table 1). The increase was caused by a simultaneous increase of diatoxanthin and diadinoxanthin (1.3- and 4.0-fold, respectively), indicating an upregulation of the

Table 1. The de-epoxidation ratio of xanthophyll cycle pigments (diatoxanthin/(diatoxanthin + diadinoxanthin)). Mean values and standard deviations (SD) of $n = 3$ are denoted. Asterisk indicates statistical significance (* represent p-value ≤ 0.05, ** represents p-value ≤ 0.01) of limitation to replete control, or in case of all replete replicates, of the two different life-cycle stages.

		De-epoxidation ratio [-]
P-starvation setup	2N replete	0.25 ± 0.11
	2N -P	0.51 ± 0.12**
	1N replete	0.25 ± 0.21
	1N -P	0.19 ± 0.03
N-starvation setup	2N replete	0.22 ± 0.05
	2N -N	0.17 ± 0.02*
	1N replete	0.28 ± 0.03
	1N -N	0.22 ± 0.04*
All replete	2N replete	0.24 ± 0.05
	1N replete	0.26 ± 0.11

xanthophyll cycle by increased diadinoxanthin production and its subsequent conversion to diatoxanthin. This has been reported to occur in *E. huxleyi* under high light stress (Harris et al. 2005; Ragni et al. 2008), as a safety mechanism, minimizing transfer of absorbed light to photosystem II reaction centers. Our results therefore suggest that, in the diploid stage, P-starvation has a similar effect on the photosynthetic apparatus as high light stress does, resulting in increased photoprotection via nonphotochemical quenching.

The triggering factor of this higher xanthophyll cycling activity is usually reactive oxygen species stress and electron pressure in the photosynthetic chain. In case of N-starvation, pigments are globally decreased, lowering light harvest and thus the overall electron load of photosynthetic chains. Under P-starvation however, overproduction of pigments even intensifies photon capture and necessitates a more intense quenching of electrons and reactive oxygen species (Phang et al. 2012; Rokitta et al. 2016). The connection between P-starvation and higher nonphotochemical quenching has been shown for *Dunaliella tertiolecta* (Petrou et al. 2008) and for rice (Xu et al. 2007). The de-epoxidation ratio was not significantly changed for the haploid life-cycle stage under P-starvation, again emphasizing the difference of these two stages, and highlighting their possible diverse niche-occupation (Houdan et al. 2005; von Dassow et al. 2009; Rokitta et al. 2011). This also explains the observed higher endurance of photosynthesis of the diploid strain under P-starvation (Rokitta et al. 2016).

In a first approximation, the increasing pigment concentrations contradict the predictions derived from the transcriptome study of Rokitta et al. (2016), who observed a down-regulation of many enzymes involved in photosynthesis, the xanthophyll cycle, as well as the synthesis of pigments,

photosystems and plastidic ATP under P-starvation. In the transcriptomic dataset, only very few transcripts were upregulated, i.e., a transcript of a fucoxanthin-chlorophyll *a-c* binding protein that protects against photooxidative stress (McKew et al. 2013). In contrast to the transcriptomic data, which indicates a general decrease of plastidic activity, here we find the functional pathways to be increased, especially in the diploid stage, leading to an overproduction of pigments as a P-starvation response. An explanation for this may be the fact that pigment production is more dependent on N than on P for precursor molecules and enzymatic machinery. Thus, the pathways are apparently functional and since N is not scarce in this situation, pigments are overproduced. This assumption is supported by the evidence of increased light harvesting proteins observed under P-starvation (McKew et al. 2015).

P-starvation led to an increase of many lipids, including polar and neutral lipid fatty acids and especially neutral storage lipids such as TAGs and alkenones, as well as alkenes, in agreement with the proposed relative increase of metabolic carbon flow through the metabolism. These results are in agreement with other studies, where total polar (McKew et al. 2015; Shemi et al. 2016), total neutral lipids (McKew et al. 2015) and alkenones (Epstein et al. 1998) increased under P-starvation, which is in line with changes in total lipids of other microalgae (Reitan et al. 1994; Zhao et al. 2009). Regarding polar lipid fatty acids, especially polyunsaturated fatty acids were increased in this study, indicating a possible increase of thylakoid membrane lipids (Fulton et al. 2014), which could be connected to the observed increase of pigment abundance. Furthermore increased coccolith production has been reported under P-starvation (Kayano and Shiraiwa 2009; Satoh et al. 2009). However, it should not require additional coccolith vesicle structures, as it results from ceased cell division, while the coccolith production continues at its usual rate (Shiraiwa 2003). The changed lipid composition under P-starvation is likely derived from the fact that cells need to dissipate photosynthate and reduction equivalents by means of lipogenesis, as is also observed in other microalgae, e.g., *Chlamydomonas reinhardtii* (Kamalanathan et al. 2016). Along with other phytoplankton, *E. huxleyi* has a highly dynamic membrane lipid composition that can be adjusted by environmental stimuli within time-frames of 1 d, e.g., replacing phospholipids with betaine lipids during P-starvation (van Mooy et al. 2009; McKew et al. 2015; Shemi et al. 2016).

The results of this study expand the knowledge of *E. huxleyi*'s success in P-limited waters (Riegman et al. 1992; Tyrrell and Taylor 1996), which include efficient scavenging of inorganic P from dissolved organic matter using alkaline phosphatases (Riegman et al. 2000) and effective budgeting of remaining P (van Mooy et al. 2009). All in all, these metabolic fingerprints of haploid and diploid *E. huxleyi* life-cycle stages confirm most transcriptome-based hypotheses related

to the central carbon metabolism, including the arrest of cell-cycling, activation of the glycolytic bypass as well as decreased mitochondrial oxidation and intensified lipid turnover. On the other side, processes like pigment synthesis and plastid activity are increased under P-starvation, because the N-containing precursors are not lacking.

This dataset is a good example of how and why transcriptomic and metabolomic assessments and derived interpretations can diverge quite strongly: The gene expression patterns triggered by cells in response to nutrient starvation appear to set the boundary conditions, the biochemical switch points. However, the instantaneous molecular fluxes and metabolic equilibria finally dominate the phenotype and thus may not be neglected. In other words, same or similar transcriptomic settings can lead to highly different phenotypes, when the precursor production and metabolite flux are different due to environmental settings.

Life-cycle stages cope differently with N-starvation

N-starvation led to slightly diverging results in both stages, suggesting a partly life-cycle stage specific response toward the starvation: While a general decrease of most assessed metabolites was found in both life cycle-stages (e.g., N-rich amino acids asparagine and glutamine), a number of investigated metabolites experienced an increase exclusively in the haploid stage, namely various carbon-rich proteinogenic amino acids and small carboxylic acids.

We found a significantly decreased abundance for adenine in the diploid stage, as well as insignificant decreases for adenosine in both stages, indicating decreased cellular nucleotide content, in agreement with results for other microalgae (Prestegard et al. 2014; Lu et al. 2016). This is in line with transcriptomic results that indicated a wider down-regulation of the synthesis pathways for nucleic acid bases under N-starvation (Rokitta et al. 2014, 2016) and also seems to be connected to the arresting of the cell cycle under nutrient starvation.

N-starvation primarily affects proteinogenic amino acids (Barsanti and Gualtieri 2006), as observed for several amino acids in the diploid stage under N-starvation. This is in line with decreased overall protein abundance, as well as increased abundance of proteins involved in degradation under N-starvation in *E. huxleyi* (McKew et al. 2015). Decreases of amino acids and protein abundance have been reported for other microalgae under N-starvation (Hockin et al. 2012; Popko et al. 2016). In the haploid stage, several amino acid abundances were increased, hinting toward life-cycle specific prioritizations of metabolic pathways. However, N-rich amino acids, such as asparagine and glutamine, were decreased in the haploid stage, indicating that N-starvation did affect this stage on level of amino acid biosynthesis.

Interestingly, N-containing proline was increased in both stages also under N-starvation, although this change was only significant in the haploid stage. These results are in agreement with the transcriptomic upregulation of the associated pathways in *E. huxleyi* life-cycle stages under nutrient starvation (Rokitta et al. 2014, 2016), and metabolite data from other unicellular eukaryotes (Onodera and Ohsumi 2005; Chokshi et al. 2017), indicating an increase of proline shortly after entering stationary phase. The findings, however, contradict results from N-starved diatoms, where proline decreased rapidly after onset of N-starvation and was suggested to be replaced as a compatible solute by increasing amounts of DMSP (Hockin et al. 2012; Popko et al. 2016). Despite different cultivation approaches used in the cited studies, a time-dependent metabolic readjustment might apply here, which certainly deserves further investigations.

As mentioned above, the high mannitol content in *E. huxleyi* is interpreted as a carbon and reductant storage in *E. huxleyi* (Obata et al. 2013; Tsuji et al. 2015). While the observed decreases of this metabolite were insignificant in both stages under P-starvation, they were significant the diploid and haploid stages under N-starvation (1.3- and 9.8-fold, respectively). Similarly, Mausz and Pohnert (2015) found a decrease of cellular mannitol content in the stationary growth phase. This suggests its use to fuel carbohydrate metabolism and to mobilize reduction equivalents like NADH to maintain redox homeostasis in the cytoplasm when photosynthetic production is decreased. As mannitol is also an important osmolyte, the decreases observed under N-starvation could possibly trigger increases in other osmolytes, as observed for DMSP and N-containing proline in the haploid stage. Stage-specific differences in coping with N-starvation could be seen in the osmolyte composition of the life-cycle stages: N-containing osmolytes, like glycine betaine and homarine, were significantly decreased or even undetectable in the diploid stage under N-starvation, while the concentration of the N-independent DMSP remained constant. In the haploid stage, glycine betaine decreased, but DMSP and homarine were significantly increased. This may be indicative of differential capabilities and prioritizations of the life-cycle stages regarding the shuttling and recycling of cellular N into different pathways. Controversial results have been reported for the DMSP abundance under N-starvation in other diploid *E. huxleyi* strains, some studies reporting increases (Turner et al. 1988) and decreases (Keller et al. 1999), while other microalgae showed increases under these conditions (Gröne and Kirst 1992; Hockin et al. 2012). DMSP has further been proposed to replace N-containing osmolytes like glycine betaine under N-starvation (Turner et al. 1988; Gröne and Kirst 1992), which is in line with our results for the haploid stage. However, it seems equally plausible that DMSP primarily functions as an antioxidant. Changed abundances could also be linked to oxidative stress under N-starvation (Stefels 2000) and thus change with light intensities or the progression of starvation as redox-active machinery is disassembled over time.

All photosynthetic pigments were found to be decreased in abundance under N-starvation in both life-cycle stages, although changes were not significant for every pigment. While fucoxanthin derivatives and diatoxanthin were decreased in both life-cycle stages, Chl c_3 and several carotenoids were significantly decreased only in the haploid stage. Decreased pigment abundance has been reported previously for *E. huxleyi* (Stolte et al. 2000; Loebl et al. 2010) and other microalgae (Li et al. 2008; Ördög et al. 2012), even though photoprotective pigments can also be increased (Mock and Kroon 2002). Missing N directly affects chlorophyll synthesis as it relies on N-containing precursors, such as glutamate (Wilhelm et al. 2006), which was significantly decreased in the diploid stage. The differences between the life-cycle stages might be related to the previously observed different photosynthetic endurance of the haploid stage, where F_v/F_m measurements showed that photosynthetic variability ceased rapidly under N-starvation (Rokitta et al. 2014). A small, but significant decrease was observed for the de-epoxidation ratio of the xanthophyll cycle in both life-cycle stages (Table 1). Due to the decrease of diadinoxanthin and diatoxanthin (2N: 1.1- and 1.5-fold, 1N: 1.4- and 2.0-fold, respectively), photoprotection via nonphotochemical quenching is not possible under -N. These data strongly suggest that flux-driven metabolome patterns rapidly manifest in the biochemical phenotype: In contrast to P-starvation, N-starvation causes a decreased metabolic flux of N-containing precursors like glutamate into the pigment-synthesizing pathways and thus has a more rapid and severe effect in the metabolic deactivation of the plastid, which was also observed under N-starvation at transcriptomic level (Rokitta et al. 2014).

N-starvation in the diploid stage led to a decrease of certain lipids, like selected TAGs, and fatty acids belonging to neutral and polar lipids, in line with decreases of total neutral and polar lipids in *E. huxleyi* reported previously (McKew et al. 2015). Increases of TAG have been observed under N-starvation, however in a different diploid strain (Malitsky et al. 2016), as well as for other microalgae (Fidalgo et al. 1998; Rodolfi et al. 2009). In both stages, $C_{18:0}$ was significantly decreased in the neutral lipid fraction, along with $C_{18:3n3}$ in the polar lipids, indicating rearrangements of lipid metabolism and turnover that were also interpreted from transcriptomic data (Rokitta et al. 2014). The effect of N-starvation on polar lipid fatty acids was more pronounced in the diploid stage, possibly indicating changes, e.g., in the thylakoid membrane composition. The diploid-specific decrease of $C_{15:0}$ indicated decreases in N-containing extraplastidial membrane lipids, as this fatty acid has been reported to be exclusively incorporated into the N-containing extraplastidial membrane lipid phosphatidylethanolamine in *E. huxleyi* (Fulton et al. 2014). However, the haploid stage massively increased its overall cellular contents of TAGs, alkenes and alkenones, emphasizing a divergent regulation of this stage regarding storage lipids.

Correlation of metabolome and transcriptome data

All in all, metabolic responses toward P- and N-starvation generally agree with the major hypotheses postulated based on transcriptomic data (Rokitta et al. 2014, 2016), with few exceptions, as described in more detail in Fig. 4. In both macronutrient starvation scenarios, the life-cycle stages of *E. huxleyi* experienced alterations in their metabolic fingerprints that were to a large extent predicted from previously obtained transcriptomic data (Rokitta et al. 2014, 2016). These alterations include, but are not restricted to the (re)cycling of amino acids (especially proline) and lipid compounds that seemingly serve as carbon and reductant stores under starvation conditions. Apart from stage-specific peculiarities, there are, however, a number of strong divergences from the transcriptomic predictions, e.g., the metabolic load of certain biochemical pathways was overcompensated under P-starvation, while it was diminished under N-starvation.

To explain these phenomena, it is interesting to consider how stress signals are integrated into the gene regulation: For example, if N is depleted, the cells would first sense this via an over-reduction of the photosynthetic electron transfer chain, because the plastidary nitrate assimilation system does no longer effectively dissipate electrons from reduced ferredoxin (Rokitta et al. 2014). P-depletion would be sensed, because ATP could no longer be synthesized, leading to a swelling H^+ gradient in the plastid (and also in the mitochondria), so that also here, an over-reduction of the electron transfer chains would be anticipated. Thus, it is highly likely that P- and N-starvation are sensed and integrated at the same points, i.e., the plastids and mitochondria. This would explain why they trigger largely the same transcriptomic responses, i.e., genetic programs that prepare the cells for growth-arrest and streamline metabolism for parsimonious element budgeting, maintaining viability and securing survival.

The quite similar transcriptomic rearrangements between both life-cycle stages and under P- and N-starvation (Rokitta et al. 2011, 2014, 2016), however, were accompanied by the manifestations of quite different phenotypes on the metabolome level. This seems to originate from the fact that N-starvation causes more widespread effects, mainly because the synthesis of nucleotides, amino acids and ultimately the operation of literally all enzymatic machinery is very N-intensive and thus severely impaired. As a result, most, if not all, biochemical processes will be negatively affected. P-starvation, however, appears to primarily affect synthesis of nucleoside-triphosphates and thus the energy budget, as well as DNA/RNA synthesis and enzyme regulation by phosphorylation. Enzymatic functionality can yet be widely preserved throughout the metabolic networks. In other words, irrespective of superordinate transcriptomic re-constellations, N-
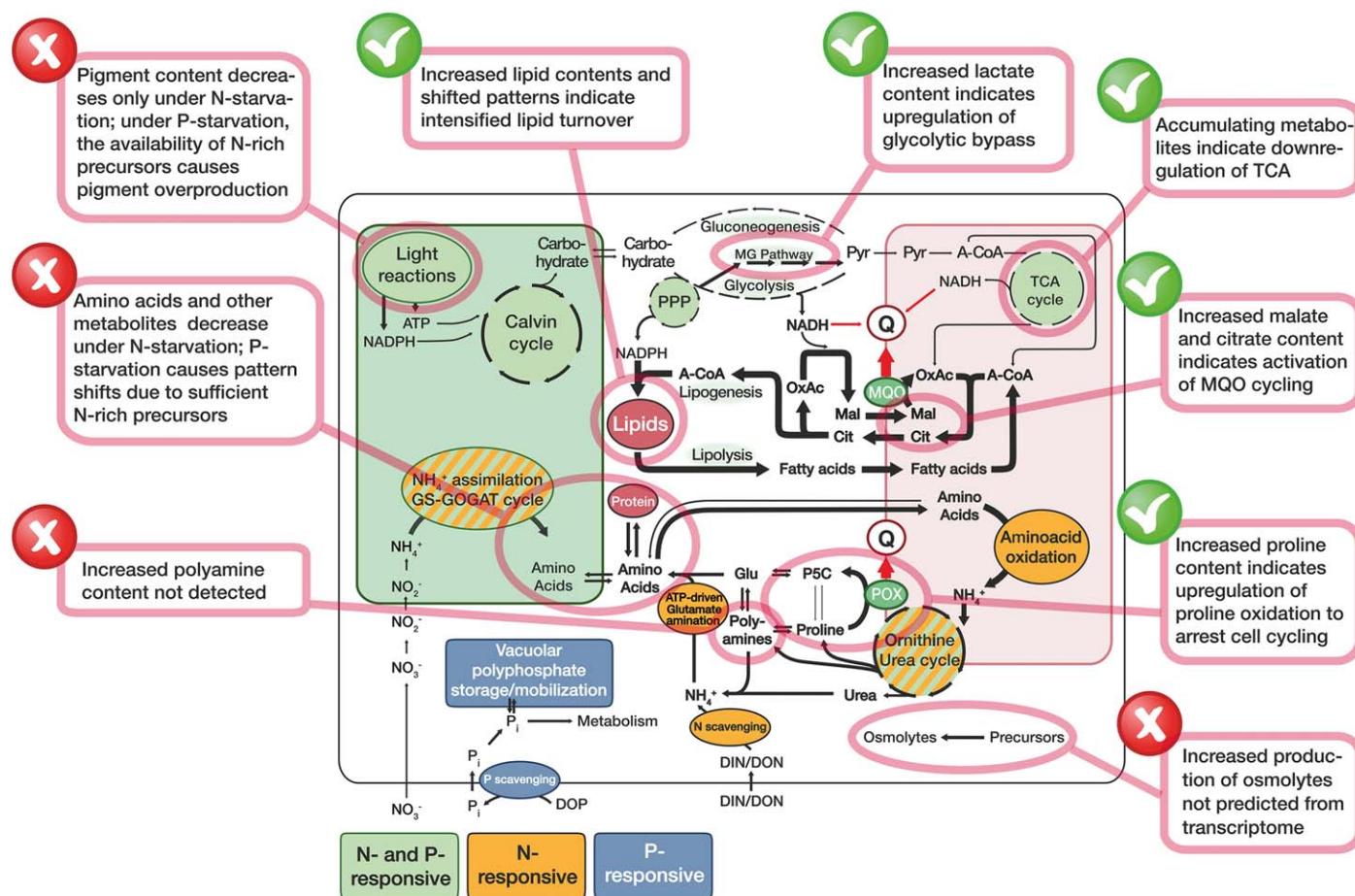
Fig. 4. Validation of a proposed schematic metabolic model of activated pathways in *E. huxleyi* (diploid and haploid cells in general) under P- and N-starvation, derived from transcriptomic data (Rokitta et al. 2016), with metabolomic data gathered in this work (text in red boxes). The schematic model proposes the following (Rokitta et al. 2016): Under nutrient-depletion, photosynthetic light reactions, and carbon fixation are minimized. As a consequence, carbon input into the cell and thus the flux through glycolysis and the TCA cycle are reduced. Cells strongly induce the citrate-shuttle that exports acetyl-CoA into the cytoplasm and increase the relative intensity of lipid turnover (synthesis as well as oxidation), which provides required sinks for reduction equivalents. To facilitate electron input into the quinone-pool (Q) under these adverse flux conditions, cells make use of a malate : quinone oxidoreductase (MQO). Mitochondrial amino acid oxidation is increased, while enzymes of the ornithine-urea-cycle (OUC) and connected reactions are throttled, putatively leading to an accumulation of OUC intermediates, polyamines, and proline relative to common amino acids. The oxidation of proline to pyrroline-5-carboxylate (P5C) by proline oxidase (POX) appears to be a major entryway for reductants into Q when nutrients are scarce and protein machinery is eroded. Especially the diploid stage induces machinery to scavenge external (in)organic N and P (orange and blue shade). See text in boxes for validation of this transcriptomic derived model with the metabolomic data of this work. Modified after Rokitta et al. (2016) under the creative common license "CC-BY 4.0." A-CoA, acetyl coenzyme A; Cit, citrate; Mal, malate; DIN/DON, dissolved inorganic/organic nitrogen; DOP, dissolved organic phosphorus; Glu, glutamic acid; GS-GOGAT, glutamine synthase-glutamine oxoglutarate aminotransferase; MG, methylglyoxal; MQO, malate-quinone-oxidoreductase; OxAc, oxaloacetate, P5C, pyrroline-5-carboxylate; POX, proline oxidase, PPP, pentose phosphate pathway; Pyr, pyruvate; Q, quinone pool; TCA, tricarboxylic acid cycle.

starvation distorts most of the cellular machinery, whereas many processes still sufficiently operate under P-starvation. Under nutrient starvation, for example, the synthesis pathways of N-rich photosynthetic pigments are generally downregulated at the transcriptomic level. However, the metabolic flux of precursors as well as the cellular enzyme content and functionality are still sufficient under P-starvation to promote high production of pigments.

These results highlight that instantaneous biochemical flux is a stronger determinant of the metabolic phenotype than the transcriptomically rearranged pathway patterns. It also shows that it is challenging to correlate and ground-truth "omics" data from different levels of biological organization with each other, as there is not necessarily a direct correlation of transcript abundance with, e.g., metabolite concentration in the corresponding pathways (Feder and Walser 2005). Due to the generic nature of some observed responses, on both the transcriptomic and metabolomic level, it may however be speculated that most microalgae can cope better and possibly longer with P-starvation than with N-starvation.

We were able to retrace the major re-constellations in biochemical pathways, find evidence for the majority of interpretations and bring up even more new hypotheses to be tested, leading to an ever emerging, and converging picture of cellular reactions toward nutrient starvation and environmental stress in general. The obtained data can help to substantiate existing metabolic models (Knies et al. 2015) and sheds more light on the evolutionary conserved reaction patterns of eukaryotic cells toward nutrient stress.

Author contributions

RW, JHM, and OK conceived and designed the experiments; RW, KC, EH, FK, KF, and JLK performed the research, with the main part of this work carried out by the first author, RW. RW and KC performed growth analysis, and all GC-MS, UV-VIS-HPLC and CAD-HPLC measurements. EH and FK conducted LC-MS/MS measurements; KF performed GC-FID measurements, and JLK conducted FTIR measurements. RW, SDR, EH, KC, FK, KF, JLK, TK, and JHM analyzed the data; RW, SDR, EH, TK, JHM, and OK wrote the paper. All authors reviewed the results and approved the final version of the manuscript.

References

Abedi, E., and M. A. Sahari. 2014. Long-chain polyunsaturated fatty acid sources and evaluation of their nutritional and functional properties. Food Sci. Nutr. **2**: 443–463. doi:10.1002/fsn3.121

Alcolombri, U., B.-D. Shifra, E. Feldmesser, Y. Levin, D. S. Tawfik, A. and Vardi. 2015. Identification of the algal dimethyl sulfide-releasing enzyme: A missing link in the marine sulfur cycle. Sci. Rep. **348**: 1466–1469. doi:10.1126/science.aab1586

Barsanti, L., and P. Gualtieri. 2006. Algae: Anatomy, biochemistry, and biotechnology. CRC Press.

Bell, M. V., and D. Pond. 1996. Lipid composition during growth of motile and coccolith forms of *Emiliania huxleyi*. Phytochemistry **41**: 465–471. doi:10.1016/0031-9422(95)00663-X

Bellou, S., and G. Aggelis. 2012. Biochemical activities in *Chlorella* sp. and *Nannochloropsis salina* during lipid and sugar synthesis in a lab-scale open pond simulating reactor. J. Biotechnol. **164**: 318–329. doi:10.1016/j.jbiotec.2013.01.010

Berges, J. A., D. J. Franklin, and P. J. Harrison. 2001. Evolution of an artificial seawater medium: Improvements in enriched seawater, artificial water over the last two decades. J. Phycol. **37**: 1138–1145. doi:10.1046/j.1529-8817.2001.01052.x

Bochenek, M., G. J. Etherington, A. Koprivova, S. T. Mugford, T. G. Bell, G. Malin, and S. Kopriva. 2013. Transcriptome analysis of the sulfate deficiency response in the marine microalga *Emiliania huxleyi*. New Phytol. **199**: 650–662. doi:10.1111/nph.12303

Bogen, C., and others. 2013. Identification of *Monoraphidium contortum* as a promising species for liquid biofuel production. Biores. Technol. **133**: 622–626. doi:10.1016/j.biortech.2013.01.164

Casetta, B., D. Tagliacozzi, B. Shushan, and G. Federici. 2000. Development of a method for rapid quantitation of amino acids by liquid chromatography-tandem mass spectrometry (LC-MSMS) in plasma. Clin. Chem. Lab. Med. **38**: 391–401. doi:10.1515/CCLM.2000.057

Chakraborty, S., K. Karmakar, and D. Chakravortty. 2014. Cells producing their own nemesis: Understanding methylglyoxal metabolism. IUBMB Life **66**: 667–678. doi:10.1002/iub.1324

Chen, W., C. Zhang, L. Song, M. Sommerfeld, and Q. Hu. 2009. A high throughput Nile red method for quantitative measurement of neutral lipids in microalgae. J. Microbiol. Methods **77**: 41–47. doi:10.1016/j.mimet.2009.01.001

Chokshi, K., I. Pancha, A. Ghosh, and S. Mishra. 2017. Nitrogen starvation-induced cellular crosstalk of ROS-scavenging antioxidants and phytohormone enhanced the biofuel potential of green microalga *Acutodesmus dimorphus*. Biotechnol. Biofuels **10**: 60. doi:10.1186/s13068-017-0747-7

Conte, M. H., A. Thompson, D. Lesley, and R. P. Harris. 1998. Genetic and physiological influences on the alkenone/alkenoate versus growth temperature relationship in *Emiliania huxleyi* and *Gephyrocapsa oceanica*. Geochim. Cosmochim. Acta **62**: 51–68. doi:10.1016/S0016-7037(97)00327-X

Dettmer, K., P. A. Aronov, and B. D. Hammock. 2007. Mass spectrometry-based metabolomics. Mass Spectrom. Rev. **26**: 51–78. doi:10.1002/mas.20108

Dewick, P. M. 2001. Medicinal natural products: A biosynthetic approach, 2nd ed. Wiley.

Dijkman, N. A., and J. C. Kromkamp. 2006. Phospholipid-derived fatty acids as chemotaxonomic markers for phytoplankton: Application for inferring phytoplankton composition. Mar. Ecol. Prog. Ser. **324**: 113–125. doi:10.3354/meps324113

Doebbe, A., M. Keck, M. La Russa, J. H. Mussgnug, B. Hankamer, E. Tekçe, K. Niehaus, and O. Kruse. 2010. The interplay of proton, electron, and metabolite supply for photosynthetic H_2 production in *Chlamydomonas reinhardtii*. J. Biol. Chem. **285**: 30247–30260. doi:10.1074/jbc.M110.122812

Dyhrman, S. T., S. T. Haley, S. R. Birkeland, L. L. Wurch, M. J. Cipriano, and A. G. McArthur. 2006. Long serial analysis of gene expression for gene discovery and transcriptome profiling in the widespread marine coccolithophore *Emiliania huxleyi*. Appl. Environ. Microbiol. **72**: 252–260. doi:10.1128/AEM.72.1.252-260.2006

Dyhrman, S. T., and others. 2012. The transcriptome and proteome of the diatom *Thalassiosira pseudonana* reveal a diverse phosphorus stress response. PLoS ONE **7**: e33768. doi:10.1371/journal.pone.0033768

Eltgroth, M. L., R. L. Watwood, and G. V. Wolfe. 2005. Production and cellular localization of neutral long-chain lipid in the haptophyte algae *Isochrysis galbana* and *Emiliania huxleyi*. J. Phycol. **41**: 1000–1009. doi:10.1111/j.1529-8817.2005.00128.x

Epstein, B. L., S. D'Hondt, J. G. Quinn, J. Zhang, and P. E. Hargraves. 1998. An effect of dissolved nutrient concentrations on alkenone-based temperature estimates. Paleoceanography **13**: 122–126. doi:10.1029/97PA03358

Escribano, M. I., and M. E. Legaz. 1988. High performance liquid chromatography of the dansyl derivatives of putrescine, spermidine, and spermine. Plant Physiol. **87**: 519–522. doi:10.1104/pp.87.2.519

Evans, C., D. W. Pond, and W. H. Wilson. 2009. Changes in *Emiliania huxleyi* fatty acid profiles during infection with *E. huxleyi* virus 86: Physiological and ecological implications. Aquat. Microb. Ecol. **55**: 219–228. doi:10.3354/ame01295

Falkowski, P. G., O. Schofield, M. E. Katz, B. van de Schootbrugge, and A. H. Knoll. 2004. Why is the land green and the ocean red? *In* H. R. Thiersteinand Jeremy R. Young [eds.], Coccolithophores: From molecular processes to global impact. Springer.

Feder, M. E., and J.-C. Walser. 2005. The biological limitations of transcriptomics in elucidating stress and stress responses. J. Evol. Biol. **18**: 901–910. doi:10.1111/j.1420-9101.2005.00921.x

Fernández, E., W. M. Balch, E. Maranon, and P. M. Holligan. 1994. High rates of lipid biosynthesis in cultured, mesocosm and coastal populations of the coccolithophore *Emiliania huxleyi*. Mar. Ecol. Prog. Ser. **117**: 13–22. doi:10.3354/meps114013

Fidalgo, J., A. Cid, E. Torres, A. Sukenik, and C. Herrero. 1998. Effects of nitrogen source and growth phase on proximate biochemical composition, lipid classes and fatty acid profile of the marine microalga *Isochrysis galbana*. Aquaculture **1166**: 105–116. doi:10.1016/S0044-8486(98)00278-6

Fiorini, S., J.-P. Gattuso, P. van Rijswijk, and J. Middelburg. 2010. Coccolithophores lipid and carbon isotope composition and their variability related to changes in seawater carbonate chemistry. J. Exp. Mar. Biol. Ecol. **394**: 74–85. doi:10.1016/j.jembe.2010.07.020

Frommolt, R., R. Goss, and C. Wilhelm. 2001. The deepoxidase and epoxidase reactions of *Mantoniella squamata* (Prasinophyceae) exhibit different substrate-specific reaction kinetics compared to spinach. Planta **213**: 446–456. doi:10.1007/s004250100589

Fulton, J. M., H. F. Fredricks, K. D. Bidle, A. Vardi, B. J. Kendrick, G. R. DiTullio, and B. A. S. Van Mooy. 2014.

Novel molecular determinants of viral susceptibility and resistance in the lipidome of *Emiliania huxleyi*. Environ. Microbiol. **16**: 1137–1149. doi:10.1111/1462-2920.12358

Garrido, J. L., J. Otero, M. A. Maestro, and M. Zapata. 2000. The main nonpolar chlorophyll c from *Emiliania huxleyi* (Prymnesiophyceae) is a chlorophyll c_2- monogalactosyldiacylglyceride ester: A mass spectrometry study. J. Phycol. **36**: 497–505. doi:10.1046/j.1529-8817.2000.99135.x

Gebser, B., and G. Pohnert. 2013. Synchronized regulation of different zwitterionic metabolites in the osmoadaption of phytoplankton. Mar. Drugs **11**: 2168–2182. doi:10.3390/md11062168

Giordano, M., M. Kansiz, P. Heraud, J. Beardall, B. Wood, and D. McNaughton. 2001. Fourier Transform Infrared Spectroscopy as a novel tool to investigate changes in intracellular macromolecular pools in the marine microalga *Chaetoceros muellerii* (Bacillariophyceae). J. Phycol. **31**: 271–279. doi:10.1046/j.1529-8817.2001.037002271.x

Gröne, T., and G. O. Kirst. 1992. The effect of nitrogen deficiency, methionine and inhibitors of methionine metabolism on the DMSP contents of *Tetraselmis subcordiformis* (Stein). Mar. Biol. **112**: 497–503. doi:10.1007/BF00356296

Han, J., S. Gagnon, T. Eckle, and C. H. Borchers. 2013. Metabolomic analysis of key central carbon metabolism carboxylic acids as their 3-nitrophenylhydrazones by UPLC/ESI-MS. Electrophoresis **34**: 2891–2900. doi:10.1002/elps.201200601

Harder, U., B. Koletzko, and W. Peissner. 2011. Quantification of 22 plasma amino acids combining derivatization and ion-pair LC–MS/MS. J. Chromatogr. B **879**: 495–504. doi:10.1016/j.jchromb.2011.01.010

Hariskos, I., M. Chairopoulou, M. Vucak, C. Posten, and U. Teipel. 2016. Production and characterization of microstructured calcite particles from the coccolithophorid alga *Emiliania huxleyi*. Chemie Ingenieur Technik **88**: 897–902. doi:10.1002/cite.201500128

Harris, G. N., D. J. Scanlan, and R. J. Geider. 2005. Acclimation of *Emiliania huxleyi* (Prymnesiophyceae) to photon flux density. J. Phycol. **41**: 851–862. doi:10.1111/j.1529-8817.2005.00109.x

Heinemann, M., and U. Sauer. 2010. Systems biology of microbial metabolism. Curr. Opin. Microbiol. **13**: 337–343. doi:10.1016/j.mib.2010.02.005

Herrgård, M. J., and others. 2008. A consensus yeast metabolic network reconstruction obtained from a community approach to systems biology. Nat. Biotechnol. **26**: 1155–1160. doi:10.1038/nbt1492

Hockin, N. L., T. Mock, F. Mulholland, S. Kopriva, and G. Malin. 2012. The response of diatom central carbon metabolism to nitrogen starvation is different from that of green algae and higher plants. Plant Physiol. **158**: 299–312. doi:10.1104/pp.111.184333

Holtz, L. M., G. Langer, S. D. Rokitta, and S. Thoms. 2013. Synthesis of nanostructured calcite particles in

coccolithophores, unicellular algae. *In* M. Rai and C. Posten [eds.], Green biosynthesis of nanoparticles. CABI.

Holtz, L.-M., D. Wolf-Gladrow, and S. Thoms. 2015. Numerical cell model investigating cellular carbon fluxes in *Emiliania huxleyi*. J. Theor. Biol. **364**: 305–315. doi:10.1016/j.jtbi.2014.08.040

Houdan, A., I. Probert, K. van Lenning, and S. Lefebvre. 2005. Comparison of photosynthetic responses in diploid and haploid life-cycle phases of *Emiliania huxleyi* (Prymnesiophyceae). Mar. Ecol. Prog. Ser. **292**: 139–146. doi:10.3354/meps292139

Hunter, J. E., M. J. Frada, H. F. Fredricks, A. Vardi, and B. A. S. Van Mooy. 2015. Targeted and untargeted lipidomics of *Emiliania huxleyi* viral infection and life cycle phases highlights molecular biomarkers of infection, susceptibility, and ploidy. Front. Mar. Sci. **2**: 367. doi:10.3389/fmars.2015.00081

Inoue, Y., K. Watanabe, M. Shimosaka, T. Saikusa, Y. Fukuda, K. Murata, and A. Kimura. 1985. Metabolism of 2-oxoaldehydes in yeasts. Eur. J. Biochem. **153**: 243–247. doi:10.1111/j.1432-1033.1985.tb09293.x

Jaeger, D., and others. 2016. Label-free *in vivo* analysis of intracellular lipid droplets in the oleaginous microalga *Monoraphidium neglectum* by coherent Raman scattering microscopy. Sci. Rep. **6**: 35340. doi:10.1038/srep35340

Jones, B. M., R. J. Edwards, P. J. Skipp, C. D. O'Connor, and M. D. Iglesias-Rodriguez. 2011. Shotgun proteomic analysis of *Emiliania huxleyi*, a marine phytoplankton species of major biogeochemical importance. Mar. Biotechnol. **13**: 496–504. doi:10.1007/s10126-010-9320-0

Jones, B. M., M. D. Iglesias-Rodriguez, P. J. Skipp, R. J. Edwards, M. J. Greaves, J. R. Young, H. Elderfield, and C. D. O'Connor. 2013. Responses of the *Emiliania huxleyi* proteome to ocean acidification. PLoS ONE **8**: e61868. doi:10.1371/journal.pone.0061868

Kamalanathan, M., M. Pierangelini, L. A. Shearman, R. Gleadow, and J. Beardall. 2016. Impacts of nitrogen and phosphorus starvation on the physiology of *Chlamydomonas reinhardtii*. J. Appl. Phycol. **28**: 1509–1520. doi:10.1007/s10811-015-0726-y

Kayano, K., and Y. Shiraiwa. 2009. Physiological regulation of coccolith polysaccharide production by phosphate availability in the coccolithophorid *Emiliania huxleyi*. Plant Cell Physiol. **50**: 1522–1531. doi:10.1093/pcp/pcp097

Keller, D. M., P. R. Kiene, A. P. Matrai, and K. W. Bellows. 1999. Production of glycine betaine and dimethylsulfoniopropionate in marine phytoplankton. I. Batch cultures. Mar. Biol. **135**: 237–248. doi:10.1007/s002270050621

Klaveness, D. 1972. *Coccolithus huxleyi* (Lohman) Kaptner. I. Morphological investigations on the vegetative cell and the process of coccolith formation. Protistologica **8**: 335–346.

Knies, D., P. Wittmüß, S. Appel, O. Sawodny, M. Ederer, and R. Feuer. 2015. Modeling and simulation of optimal resource management during the diurnal cycle in *Emiliania huxleyi* by genome-scale reconstruction and an extended flux balance analysis approach. Metabolites **5**: 659–676. doi:10.3390/metabo5040659

Knothe, G., S. C. Cermak, and R. L. Evangelista. 2009. Cuphea oil as source of biodiesel with improved fuel properties caused by high content of methyl decanoate. Energy Fuels **23**: 1743–1747. doi:10.1021/ef800958t

Kobayashi, K., K. Endo, and H. Wada. 2016. Roles of lipids in photosynthesis. *In* Y. Nakamura and Yonghua Li-Beisson [eds.], Lipids in plant and algae development. Springer International Publishing.

Kopka, J., and others. 2005. GMD@CSB.DB: The Golm Metabolome Database. Bioinformatics **21**: 1635–1638. doi:10.1093/bioinformatics/bti236

Kottmeier, D. M., S. D. Rokitta, and B. Rost. 2016. Acidification, not carbonation, is the major regulator of carbon fluxes in the coccolithophore *Emiliania huxleyi*. New Phytol. **211**: 126–137. doi:10.1111/nph.13885

Kozlowska-Szerenos, B., I. Bialuk, and S. Maleszewski. 2004. Enhancement of photosynthetic O_2 evolution in *Chlorella vulgaris* under high light and increased CO_2 concentration as a sign of acclimation to phosphate deficiency. Plant Physiol. Biochem. **42**: 403–409. doi:10.1016/j.plaphy.2004.02.010

Krumov, N., and C. Posten. 2013. Nanostructured particles from coccolithophores - an undiscovered resource for applications. *In* M. Rai and C. Posten [eds.], Green biosynthesis of nanoparticles. CABI.

Li, Y., M. Horsman, B. Wang, N. Wu, and C. Q. Lan. 2008. Effects of nitrogen sources on cell growth and lipid accumulation of green alga *Neochloris oleoabundans*. Appl. Microbiol. Biotechnol. **81**: 629–636. doi:10.1007/s00253-008-1681-1

Llewellyn, C. A., C. Evans, R. L. Airs, I. Cook, N. Bale, and W. H. Wilson. 2007. The response of carotenoids and chlorophylls during virus infection of *Emiliania huxleyi* (Prymnesiophyceae). J. Exp. Mar. Biol. Ecol. **344**: 101–112. doi:10.1016/j.jembe.2006.12.013

Loebl, M., A. M. Cockshutt, D. A. Campbell, and A. Z V. Finkel. 2010. Physiological basis for high resistance to photoinhibition under nitrogen depletion in *Emiliania huxleyi*. Limnol. Oceanogr. **55**: 2150–2160. doi:10.4319/lo.2010.55.5.2150

Lu, N., J.-H. Chen, D. Wei, F. Chen, and G. Chen. 2016. Global metabolic regulation of the snow alga *Chlamydomonas nivalis* in response to nitrate or phosphate deprivation by a metabolome profile analysis. Int. J. Mol. Sci. **17**: 694. doi:10.3390/ijms17050694

Malitsky, S., and others. 2016. Viral infection of the marine alga *Emiliania huxleyi* triggers lipidome remodeling and induces the production of highly saturated triacylglycerol. New Phytol. **210**: 88–96. doi:10.1111/nph.13852

Martins, D. A., L. Custodio, L. Barreira, H. Pereira, R. Ben-Hamadou, J. Varela, and K. M. Abu-Salah. 2013.

Alternative sources of n-3 long-chain polyunsaturated fatty acids in marine microalgae. Mar. Drugs **11**: 2259–2281. doi:10.3390/md11072259

Mausz, M. A., and G. Pohnert. 2015. Phenotypic diversity of diploid and haploid *Emiliania huxleyi* cells and of cells in different growth phases revealed by comparative metabolomics. J. Plant Physiol. **172**: 137–148. doi:10.1016/j.jplph.2014.05.014

McKew, B. A., and others. 2013. The trade-off between the light-harvesting and photoprotective functions of fucoxanthin-chlorophyll proteins dominates light acclimation in *Emiliania huxleyi* (clone CCMP 1516). New Phytol. **200**: 74–85. doi:10.1111/nph.12373

McKew, B. A., G. Metodieva, C. A. Raines, M. V. Metodiev, and R. J. Geider. 2015. Acclimation of *Emiliania huxleyi* (1516) to nutrient limitation involves precise modification of the proteome to scavenge alternative sources of N and P. Environ. Microbiol. **17**: 4050–4062. doi:10.1111/1462-2920.12957

Mock, T., and B. M. Kroon. 2002. Photosynthetic energy conversion under extreme conditions - I: Important role of lipids as structural modulators and energy sink under N-limited growth in Antarctic sea ice diatoms. Phytochemistry **1**: 41–51. doi:10.1016/S0031-9422(02)00216-9

Naumann, D. 2001. FT-Infrared and FT-Raman Spectroscopy in biomedical research. Appl. Spectrosc. Rev. **36**: 239–298. doi:10.1081/ASR-100106157

Obata, T., S. Schoenefeld, I. Krahnert, S. Bergmann, A. Scheffel, and A. R. Fernie. 2013. Gas-chromatography mass-spectrometry (GC-MS) based metabolite profiling reveals mannitol as a major storage carbohydrate in the coccolithophorid alga *Emiliania huxleyi*. Metabolites **3**: 168–184. doi:10.3390/metabo3010168

Onodera, J., and Y. Ohsumi. 2005. Autophagy is required for maintenance of amino acid levels and protein synthesis under nitrogen starvation. J. Biol. Chem. **280**: 31582–31586. doi:10.1074/jbc.M506736200

Ördög, V., W. A. Stirk, P. Bálint, J. van Staden, and C. Lovász. 2012. Changes in lipid, protein and pigment concentrations in nitrogen-stressed *Chlorella minutissima* cultures. J. Appl. Phycol. **24**: 907–914. doi:10.1007/s10811-011-9711-2

Paasche, E. 1998. Roles of nitrogen and phosphorus in coccolith formation in *Emiliania huxleyi* (Prymnesiophyceae). Eur. J. Phycol. **33**: 33–42. doi:10.1017/S0967026297001480

Paasche, E. 2001. A review of the coccolithophorid *Emiliania huxleyi* (Prymnesiophyceae), with particular reference to growth, coccolith formation, and calcification-photosynthesis interactions. Phycologia **40**: 503–529. doi:10.2216/i0031-8884-40-6-503.1

Pelusi, A., Y. Hanawa, H. Araie, I. Suzuki, M. Giordano, and Y. Shiraiwa. 2016. Rapid detection and quantification of haptophyte alkenones by Fourier transform infrared spectroscopy (FTIR). Algal Res. **19**: 48–56. doi:10.1016/j.algal.2016.07.006

Petrou, K., M. A. Doblin, R. A. Smith, P. J. Ralph, K. Shelly, and J. Beardall. 2008. State transitions and nonphotochemical quenching during a nutrient-induced fluorescence transient in phosphorus-starved *Dunaliella tertiolecta*. J. Phycol. **44**: 1204–1211. doi:10.1111/j.1529-8817.2008.00585.x

Phang, J. M., W. Liu, C. Hancock, and K. J. Christian. 2012. The proline regulatory axis and cancer. Front. Oncol. **2**: 1–12. doi:10.3389/fonc.2012.00060

Pond, D. W., and R. P. Harris. 1996. The lipid composition of the coccolithophore *Emiliania huxleyi* and its possible ecophysiological significance. J. Mar. Biol. Assoc. UK **76**: 579–594. doi:10.1017/S0025315400031295

Popko, J., and others. 2016. Metabolome analysis reveals betaine lipids as major source for triglyceride formation, and the accumulation of sedoheptulose during nitrogen-starvation of *Phaeodactylum tricornutum*. PLoS ONE **11**: e0164673. doi:10.1371/journal.pone.0164673

Prestegard, S. K., G. Knutsen, and L. Herfindal. 2014. Adenosine content and growth in the diatom *Phaeodactylum tricornutum* (Bacillariophyceae): Effect of salinity, light, temperature and nitrate. Diatom Res. **29**: 361–369. doi:10.1080/0269249X.2014.889040

Ragni, M., R. L. Airs, N. Leonardos, and R. J. Geider. 2008. Photoinhibition of PSII in *Emiliania huxleyi* (Haptophyta) under high light stress: The roles of photoacclimation, photoprotection, and photorepair. J. Phycol. **44**: 670–683. doi:10.1111/j.1529-8817.2008.00524.x

Read, B. A., and others. 2013. Pan genome of the phytoplankton *Emiliania* underpins its global distribution. Nature **499**: 209–213. doi:10.1038/nature12221

Reitan, K. I., J. R. Rainuzzo, and Y. Olsen. 1994. Effect of nutrient limitation on fatty acid and lipid content of marine microalgae. J. Phycol. **30**: 972–979. doi:10.1111/j.0022-3646.1994.00972.x

Riebesell, U., I. Zondervan, B. Rost, P. D. Tortell, R. E. Zeebe, and F. M. M. Morel. 2000. Reduced calcification of marine plankton in response to increased atmospheric CO_2. Nature **407**: 364–367. doi:10.1038/35030078

Riegman, R., A. A. M. Noordeloos, and G. C. Cadée. 1992. *Phaeocystis* blooms and eutrophication of the continental coastal zones of the North Sea. Mar. Biol. **112**: 479–484. doi:10.1007/BF00356293

Riegman, R., W. Stolte, A. A. M. Noordeloos, and D. Slezak. 2000. Nutrient uptake and alkaline phosphatase (ec 3:1:3:1) activity of *Emiliania huxleyi* (Prymnesiophyceae) during growth under N and P limitation in continuous cultures. J. Phycol. **36**: 87–96. doi:10.1046/j.1529-8817.2000.99023.x

Rodolfi, L., G. Chini Zittelli, N. Bassi, G. Padovani, N. Biondi, G. Bonini, and M. R. Tredici. 2009. Microalgae for oil: Strain selection, induction of lipid synthesis and outdoor mass cultivation in a low-cost photobioreactor. Biotechnol. Bioeng. **102**: 100–112. doi:10.1002/bit.22033

Rokitta, S. D., L. J. de Nooijer, S. Trimborn, C. de Vargas, B. Rost, and U. John. 2011. Transcriptome analyses reveal

differential gene expression patterns between the life-cycle stages of *Emiliania huxleyi* (Haptophyta) and reflect specialization to different ecological niches. J. Phycol. **47**: 829–838. doi:10.1111/j.1529-8817.2011.01014.x

Rokitta, S. D., and B. Rost. 2012. Effects of CO_2 and their modulation by light in the life-cycle stages of the coccolithophore *Emiliania huxleyi*. Limnol. Oceanogr. **57**: 607–618. doi:10.4319/lo.2012.57.2.0607

Rokitta, S. D., P. von Dassow, B. Rost, and U. John. 2014. *Emiliania huxleyi* endures N-limitation with an efficient metabolic budgeting and effective ATP synthesis. BMC Genomics **15**: 1051. doi:10.1186/1471-2164-15-1051

Rokitta, S. D., P. von Dassow, B. Rost, and U. John. 2016. P- and N-depletion trigger similar cellular responses to promote senescence in eukaryotic phytoplankton. Front. Mar. Sci. **3**: 1–13. doi:10.3389/fmars.2016.00109

Rosenwasser, S., and others. 2014. Rewiring host lipid metabolism by large viruses determines the fate of *Emiliania huxleyi*, a bloom-forming alga in the ocean. Plant Cell **26**: 2689–2707. doi:10.1105/tpc.114.125641

Rost, B., and U. Riebesell. 2004. Coccolithophores and the biological pump: Responses to environmental changes. *In* H. R. Thierstein and Jeremy R. Young [eds.], Coccolithophores: From molecular processes to global impact. Springer.

Sarazin, G., G. Michard, and F. Prevot. 1999. A rapid and accurate spectroscopic method for alkalinity measurements in sea water samples. Water Res. **33**: 290–294. doi:10.1016/S0043-1354(98)00168-7

Satoh, M., K. Iwamoto, I. Suzuki, and Y. Shiraiwa. 2009. Cold stress stimulates intracellular calcification by the coccolithophore, *Emiliania huxleyi* (Haptophyceae) under phosphate-deficient conditions. Mar. Biotechnol. **11**: 327–333. doi:10.1007/s10126-008-9147-0

Sawada, K., N. Handa, Y. Shiraiwa, A. Danbara, and S. Montani. 1996. Long-chain alkenones and alkyl alkenoates in the coastal and pelagic sediments of the northwest North Pacific, with special reference to the reconstruction of *Emiliania huxleyi* and *Gephyrocapsa oceanica* ratios. Org. Geochem. **24**: 751–764. doi:10.1016/S0146-6380(96)00087-3

Sawada, K., and Y. Shiraiwa. 2004. Alkenone and alkenoic acid compositions of the membrane fractions of *Emiliania huxleyi*. Phytochemistry **65**: 1299–1307. doi:10.1016/j.phytochem.2004.03.015

Sayanova, O., R. P. Haslam, M. Venegas Calerón, N. Ruiz López, C. Worthy, P. Rooks, M. J. Allen, and J. A. Napier. 2011. Identification and functional characterisation of genes encoding the omega-3 polyunsaturated fatty acid biosynthetic pathway from the coccolithophore *Emiliania huxleyi*. Phytochemistry **72**: 594–600. doi:10.1016/j.phytochem.2011.01.022

Shemi, A., D. Schatz, H. F. Fredricks, B. A. S. Van Mooy, Z. Porat, and A. Vardi. 2016. Phosphorus starvation induces membrane remodeling and recycling in *Emiliania huxleyi*. New Phytol. **211**: 886–898. doi:10.1111/nph.13940

Shiraiwa, Y. 2003. Physiological regulation of carbon fixation in the photosynthesis and calcification of coccolithophorids. Comp. Biochem. Physiol. B Biochem. Mol. Biol. **136**: 775–783. doi:10.1016/S1096-4959(03)00221-5

Spielmeyer, A., B. Gebser, and G. Pohnert. 2011. Dimethylsulfide sources from microalgae: Improvement and application of a derivatization-based method for the determination of dimethylsulfoniopropionate and other zwitterionic osmolytes in phytoplankton. Mar. Chem. **124**: 48–56. doi:10.1016/j.marchem.2010.12.001

Stefels, J. 2000. Physiological aspects of the production and conversion of DMSP in marine algae and higher plants. J. Sea Res. **43**: 183–197. doi:10.1016/S1385-1101(00)00030-7

Stehfest, K., J. Toepel, and C. Wilhelm. 2005. The application of micro-FTIR spectroscopy to analyze nutrient stress-related changes in biomass composition of phytoplankton algae. Plant Phys. Biochem. **43**: 717–726. doi:10.1016/j.plaphy.2005.07.001

Stolte, W., G. W. Kraay, A. A. M. Noordeloos, and R. Riegman. 2000. Genetic and physiological variation in pigment composition of *Emiliania huxleyi* (Prymnesiophyceae) and the potential use of its pigment ratios as a quantitative physiological marker. J. Phycol. **36**: 529–539. doi:10.1046/j.1529-8817.2000.99158.x

Sumner, L. W., and others. 2007. Proposed minimum reporting standards for chemical analysis. Metabolomics **3**: 211–221. doi:10.1007/s11306-007-0082-2

Sunda, W., D. J. Kieber, R. P. Kiene, and S. Huntsman. 2002. An antioxidant function for DMSP and DMS in marine algae. Nature **418**: 317–320. doi:10.1038/nature00851

Sviben, S., and others. 2016. A vacuole-like compartment concentrates a disordered calcium phase in a key coccolithophorid alga. Nat. Commun. **7**: 11228. doi:10.1038/ncomms11228

Theodorou, M. E., I. R. Elrifi, D. H. Turpin, and W. C. Plaxton. 1991. Effects of phosphorus limitation on respiratory metabolism in the green alga *Selenastrum minutum*. Plant Physiol. **95**: 1089–1095. doi:10.1104/pp.95.4.1089

Tsuji, Y., M. Yamazaki, I. Suzuki, and Y. Shiraiwa. 2015. Quantitative analysis of carbon flow into photosynthetic products functioning as carbon storage in the marine coccolithophore, *Emiliania huxleyi*. Mar. Biotechnol. **17**: 428–440. doi:10.1007/s10126-015-9632-1

Turner, S. M., G. Malin, P. S. Liss, D. S. Harbour, and P. M. Holligan. 1988. The seasonal variation of dimethyl sulfide and dimethylsulfoniopropionate concentrations in nearshore waters. Limnol. Oceanogr. **33**: 364–375. doi:10.4319/lo.1988.33.3.0364

Tyrrell, T., and A. Taylor. 1996. A modelling study of *Emiliania huxleyi* in the NE atlantic. J. Mar. Syst. **9**: 83–112. doi:10.1016/0924-7963(96)00019-X

van Mooy, B. A., and others. 2009. Phytoplankton in the ocean use non-phosphorus lipids in response to phosphorus scarcity. Nature **458**: 69–72. doi:10.1038/nature07659

van Wagenen, J., T. W. Miller, S. Hobbs, P. Hook, B. Crowe, and M. Huesemann. 2012. Effects of light and temperature on fatty acid production in *Nannochloropsis salina*. Energies **5**: 731–740. doi:10.3390/en5030731

Volkman, J. K., G. Eglinton, E. D. Corner, and T. Forsberg. 1980. Long-chain alkenes and alkenones in the marine coccolithophorid *Emiliania huxleyi*. Phytochemistry **19**: 2619–2622. doi:10.1016/S0031-9422(00)83930-8

Volkman, J. K., D. J. Smith, G. Eglinton, T. E. V. Forsberg, and E. D. S. Corner. 1981. Sterol and fatty acid composition of four marine haptophycean algae. J. Mar. Biol. Assoc. UK **61**: 509. doi:10.1017/S0025315400047111 doi: 10.1017/S0025315400047111

Volkman, J. K., D. A. Everitt, and D. I. Allen. 1986. Some analyses of lipid classes in marine organisms, sediments and seawater using thin-layer chromatography-flame ionisation detection. J. Chromatogr. A **356**: 147–162. doi: 10.1016/S0021-9673(00)91474-2

von Dassow, P., H. Ogata, I. Probert, P. Wincker, S. C. Da, S. Audic, J. M. Claverie, and C. de Vargas. 2009. Transcriptome analysis of functional differentiation between haploid and diploid cells of *Emiliania huxleyi*, a globally significant photosynthetic calcifying cell. Genome Biol. **10**: R114. doi:10.1186/gb-2009-10-10-r114

von Dassow, P., and others. 2015. Life-cycle modification in open oceans accounts for genome variability in a cosmopolitan phytoplankton. ISME J. **9**: 1365–1377. doi: 10.1038/ismej.2014.221

Wilhelm, C., and others. 2006. The regulation of carbon and nutrient assimilation in diatoms is significantly different from green algae. Protist **157**: 91–124. doi:10.1016/j.protis.2006.02.003

Wilson, W. H., S. Turner, and N. H. Mann. 1998. Population dynamics of phytoplankton and viruses in a phosphate-limited mesocosm and their effect on DMSP and DMS production. Estuar. Coast. Shelf Sci. **46**: 49–59. doi: 10.1006/ecss.1998.0333

Wurch, L. L., E. M. Bertrand, M. A. Saito, B. A. S. Van Mooy, and S. T. Dyhrman. 2011. Proteome changes driven by phosphorus deficiency and recovery in the brown tide-forming alga *Aureococcus anophagefferens*. PLoS ONE **6**: e28949. doi:10.1371/journal.pone.0028949

Xu, H. X., X. Y. Weng, and Y. Yang. 2007. Effect of phosphorus deficiency on the photosynthetic characteristics of rice plants. Russ. J. Plant Physiol. **54**: 741–748. doi: 10.1134/S1021443707060040

Young, J. R., S. A. Davis, P. R. Bown, and S. Mann. 1999. Coccolith ultrastructure and biomineralisation. J. Struct. Biol. **126**: 195–215. doi:10.1006/jsbi.1999.4132

Zeebe, R. E., and D. A. Wolf-Gladrow. 2001. CO_2 in seawater: Equilibrium, kinetics, isotopes, 1st ed. Elsevier Science.

Zhang, X., J. Gamarra, S. Castro, E. Carrasco, A. Hernandez, T. Mock, A. R. Hadaegh, and B. A. Read. 2016. Characterization of the small RNA transcriptome of the marine coccolithophorid, *Emiliania huxleyi*. PLoS ONE **11**: e0154279. doi:10.1371/journal.pone.0154279

Zhao, Y., Z. Yu, X. Song, and X. Cao. 2009. Biochemical compositions of two dominant bloom-forming species isolated from the Yangtze River estuary in response to different nutrient conditions. J. Exp. Mar. Biol. Ecol. **368**: 30–36. doi:10.1016/j.jembe.2008.09.023

Conflict of Interest

None declared.